Curated Pacific Northwest AI-ready Seismic Dataset

Yiyu Ni [1*], Alexander R. Hutko [1,2], Francesca Skene [1], Marine A. Denolle [1], Stephen D. Malone [1,2], Paul Bodin[1,2], J. Renate Hartog [1,2], Amy K. Wright [1,2]

[1)] Department of Earth and Space Sciences, University of Washington, Seattle, WA

[2)] Pacific Northwest Seismic Network, Seattle, WA

* corresponding author: niyiyu@uw.edu

Non-peer reviewed preprint submitted to *EarthArXiv*. It is in the process of reviewing of *Seismica*

Curated Pacific Northwest AI-ready Seismic Dataset

Yiyu Ni [*1], **Alexander R. Hutko** [1,2], **Francesca Skene** [1], **Marine A. Denolle** [1], **Stephen D. Malone** [1,2], **Paul Bodin** [1,2], **J. Renate Hartog** [1,2], **Amy K. Wright** [1,2]

[1]Department of Earth and Space Sciences, University of Washington, Seattle, WA, [2]Pacific Northwest Seismic Network, Seattle, WA

Author contributions: *Conceptualization*: YN, MD. *Methodology*: YN, MD, AH. *Software*: YN. *Validation*: YN, AW, RH, AH, SM, PB. *Formal analysis*: YN. *Investigation*: YN, MD. *Resources*: MD. *Writing - original draft*: YN. *Writing - review & editing*: YN, MD, AH, RH, AW, SM, FS, PB. *Visualization*: YN, MD. *Supervision*: MD, SM. *Project administration*: MD. *Funding acquisition*: MD, RH.

Abstract The curation of seismic data sets is the cornerstone of seismological research and the starting point of machine-learning applications in seismology. We present a 21-year-long AI-ready data set of diverse seismic event parameters, instrumentation metadata, and waveforms, as curated by the Pacific Northwest Seismic Network and ourselves. We describe the earthquake catalog and the temporal evolution of the data attributes (e.g., event magnitude type, channel type, waveform polarity, and signal-to-noise ratio, phase picks) as the network earthquake monitoring system evolved through time. We propose this AI-ready data set as a new open-source benchmark data set.

Non-technical summary AI-ready data sets have been the primary drivers for developing machine learning algorithms. The diversity of the data these models are trained from is a leading factor for model performance and the potential for extrapolation or generalization. This work presents a curated AI-ready data set of seismic events that were generated and recorded in the Pacific Northwest of the United States. The data set contains metadata curated by the Pacific Northwest Seismic Network and waveforms from typical earthquakes, but also human-generated quarry blasts and sonic booms, and surface processes such as snow avalanches.

1 Introduction

The Pacific Northwest (PNW) region of the United States is a dynamic tectonic plate boundary between the North American continental plate and the Juan de Fuca oceanic plate. The active margin between the two plates is a subduction zone that hosts a wide variety of earthquake behaviors: fast and large megathrust earthquakes (Witter et al., 2003), intraslab earthquakes (Gene A. Ichinose, 2004), crustal earthquakes (Gomberg and Bodin, 2021), slow repeating earthquakes (Rogers and Dragert, 2003; Wech and Bartlow, 2014; Bartlow, 2020), tectonic tremor (Wech et al., 2010), and low-frequency events (A.A.Royer and M.G.Bostock, 2014). The PNW has over twenty active volcanoes that have experienced eruptions in the historical record. The PNW has hundreds of glaciers in the Cascades, the Olympic Peninsula, and sitting atop the Cascade Volcanoes. Due to the active tectonics and the particular mid-latitude climate, the PNW also experiences hundreds of landslides every year (Luna and Korup, 2022). Such geohazards generate seismic waves that are well recorded (Allstadt, 2013; Allstadt et al., 2018a; Hibert et al., 2019).

The Pacific Northwest Seismic Network (PNSN) is the authoritative seismic network in the states of Washington and Oregon as part of the Advanced National Seismic System (ANSS), which is coordinated by the United States Geological Survey (USGS). PNSN started in 1969 with 5 seismometers and has more than 600 active seismic stations as of 1 November 2022. The authoritative boundaries of the seismic network are geographical (see Figure 3), but the Cascadia subduction zone is also active in Northern California and southern British Columbia (Ducellier and Creager, 2022; Dragert et al., 2001). The longevity of the seismic records and the richness of the active geohazards in the PNW form a unique opportunity to explore a vast range of seismic signatures. Comprehensive investigations that relate seismic signature to specific geohazards (Braun et al., 2020; Feng, 2012; Allstadt et al., 2018b; Hibert et al., 2019) benefit from curated data sets.

In recent years, machine learning has increasingly been used for applications in geosciences and seismology in particular. The rise of machine learning, especially deep learning, is largely due to the curation of several computer vision (ImageNet, Deng et al., 2009) and natural language processing (GLUE, Wang et al., 2018) data sets. There is a clear surge of machine-learning workflows in seismological research (Kong et al., 2019; Malfante et al., 2018; Bergen

*Corresponding author: niyiyu@uw.edu

et al., 2019; Mousavi and Beroza, 2022) that is driven by the high dimensionality of seismological data, the dramatic growth in data volumes (Hutko et al., 2017), and the effort by the community to curate seismic data sets. There exists today several curated data sets that have become standards for machine-learning seismological research: STEAD- a data set of local and regional earthquakes and high-frequency noise recorded globally (STanford EArthquake Dataset, Mousavi et al., 2019), INSTANCE (Italian seismic data set for machine learning, Michelini et al., 2021), ETHZ (Eidgenössische Technische Hochschule Zürich, Woollam et al., 2022), SCEDC (Southern California Earthquake Data Center, SCEDC, 2013), and Iquique- a data collection of subduction-zone earthquakes and regional recordings (Woollam et al., 2019). These data sets contain earthquake and noise time series recorded by various seismometers. The typical data attributes are basic earthquake source and receiver characteristics, including locations, magnitudes, focal mechanisms, and waveforms. The majority of the earthquake sources in these data sets are of tectonic origins: transform plate boundaries such as in California, subduction zone, and intra-continental crustal earthquakes (Woollam et al., 2019; Michelini et al., 2021). Such data sets are considered "AI-ready" since their data and attributes are packaged in data formats commonly used by the Machine Learning community.

Surface processes may also generate seismic waves. Environmental seismology is a blooming field that utilizes seismic waves to understand surface and environmental processes. There is a body of research done on the seismic signatures of landslides events (Chmiel et al., 2021; Yan et al., 2020; Hibert et al., 2014), avalanche signals (Braun et al., 2020), and debris flows (Chmiel et al., 2021), most of which investigate specific case studies. Catalogs of such events are available in the Incorporated Research Institutions for Seismology (IRIS) Exotic Seismic Event Catalog (ESEC) (e.g., Allstadt et al., 2017; Bahavar et al., 2019; Collins et al., 2022); these refined and ground-truth catalogs only contain a few ($\sim$100) events.

Our study provides a novel curated AI-ready data set of event and waveform data for a diverse range of short-duration seismic sources that include tectonic earthquakes, explosions, surface events such as ice/rock falls and avalanches, sonic booms, and thunderstorms. Not included are phenomena such as non-volcanic tremors or low amplitude low-frequency earthquakes (LFEs). We leverage the 21 years of data curation by the PNSN seismic analysts and researchers to measure the event P- and S-phase arrival times and other attributes. To enable optimal re-usability of our data set for machine learning studies, we organized the data set using the SeisBench data format (Woollam et al., 2022). We acknowledge the accompanying human biases that often pollute AI-ready data sets (Paullada et al., 2021) are well present in our catalog of event and waveform attributes. Some of these identified biases are discussed below and are obvious topics of future investigations.

2 Data Selection and Preparation

The PNSN has been monitoring the seismicity in the PNW since 1969. However, seismic waveform data from PNSN were recorded on film and paper until 1980, when digital data became available. From 1980 to 2002, event-triggered waveform data (often with a limited duration) were saved, but continuous archiving did not start until 2002. For machine-learning applications, long seismic traces as input data are preferred to allow user flexibility when trimming and shifting the data in future investigations (e.g., data augmentation (Zhu et al., 2020)). The data must also have the same dimensions, i.e., the same number of samples. To get waveforms that are long enough (i.e., 150 seconds and longer in this study), we start the curation when continuous data are available from IRIS Data Management Center (DMC) since 2002. The drawback of this choice is that it excludes the largest tectonic earthquakes in the region because they occurred before 2002 (e.g., Nisqually Earthquake of 28 February 2001). In addition, we require that both a P-wave arrival time and an S-wave arrival time information are available for the same station for each event. This requirement removes some of the smaller, older earthquakes for which no S-picks were available. In the context of AI-ready data sets, the associated metadata (labels or attributes) include event-derived parameters, station parameters, and waveform parameters. We use the SeisBench metadata format: Table 2 lists the attributes that we associate with each set of waveforms.

2.1 Event Parameters

The detection of new events is both automated and manually reviewed by the regional seismic network staff. The PNSN monitors and reports on the seismicity in the region using data from seismic stations. A trigger at a station occurs when the short-term-average-long-time-average of the seismic data (STA/LTA, Allen (1982)) exceeds a threshold. When a few stations from a designated geospatial group of seismic stations, called a subnet, experience a trigger, events are automatically saved. The PNSN analysts review all automatically detected events and remove erroneous ones by visual inspection of the event waveforms, a process they refer to as "trigger review". Teleseisms are also identified but not further processed.

If the waveform has a clear but emergent signal, does not contain distinct P and S arrivals, and the frequency content is relatively low, the PNSN assigns a "surface event" label (su) to the source type. Most surface events are "ice" quakes or avalanches associated with glaciers in the Cascades and on the volcanoes; however, some may be debris flows or rock falls. Other non-earthquake phenomena occasionally saved by analysts are recordings of sonic booms, thunderstorms, and other "interesting" events. Such waveforms are picked at very few nearby stations (one or two), and we gather the phase pick information in a catalog that we refer to as the "Exotic Event" catalog.

Once the trigger review identifies an event as an actual earthquake, the PNSN analysts further process the data. First, the automated system picks the arrival times of seismic phases from the recorded seismograms, which are one of the most important and primary data products extracted from the raw waveforms. The analyst reviews and modifies the picks.

Seismic phase picking is the cornerstone of seismological research. With accurate phase arrival information, the analysts can locate the event and estimate its origin time. At the PNSN, the first P- and S-waves are the phases picked for local and regional events. As a part of the PNSN's ANSS Quake Monitoring System (AQMS), the network analysts use Jiggle, a graphical user interface in Java to pick arrivals, locate events, and recalculate magnitudes (Hartog et al., 2019). The analysts will manually annotate the arrival time and estimate the uncertainties of their picks. The phase arrivals are only picked on a single component per station, with P-waves usually picked on vertical channels (Z component) and S-waves on horizontal channels (E/N or 1/2 components). When it is clear, the polarity (first motion is up–positive–, or down –negative–) of the P-phase is labeled by the analyst as well. Both acceleration and velocity channels are used for phase picking, although velocity channels are the most commonly used. The PNSN operates sites with both velocity channels (broad-band or short-period high-gain seismometers) and acceleration channels (low-gain accelerometers used for "strong motion" seismology). Velocity channels are preferred when both instrument types exist since they usually have a higher signal-to-noise ratio than the strong-motion channel.

Additional earthquake characteristics may be obtained from the phase polarity and amplitudes, such as focal mechanisms and magnitudes. All event parameters are saved in PNSN's AQMS database, and reasonably well-located earthquakes and explosions are reported to the ANSS Comprehensive Earthquake Catalog (ComCat, Survey, 2017) via USGS Product Distribution Layer (PDL), the software-server infrastructure that all the ANSS regional networks use to distribute earthquake products. It is important to note that the combination of automated tools, which get updated through time, and manual intervention renders the event parameters not statistically stationary over time.

This study splits the PNW catalog into several data sets: one that has PNSN analyst-verified event attributes that were sent to the USGS, which we refer to as the "ComCat event" data set, one that we refer to as the "exotic event" data set and that has remained internal in the PNSN AQMS database, and one that focuses on the 2022 Northern California earthquake sequence. These data sets are packaged in different files because they have different window lengths and data attributes. We collect and organize the data from these. We show in Figure 1 the annual event counts for the two sets of events, ComCat and exotic, that are selected for the curated data set. The temporal patterns ought not to be interpreted as changes in seismicity rate since there are systematic biases in the detection and labeling of the events through time, whether they are human (analyst) or instrumental (increased instrumental coverage).

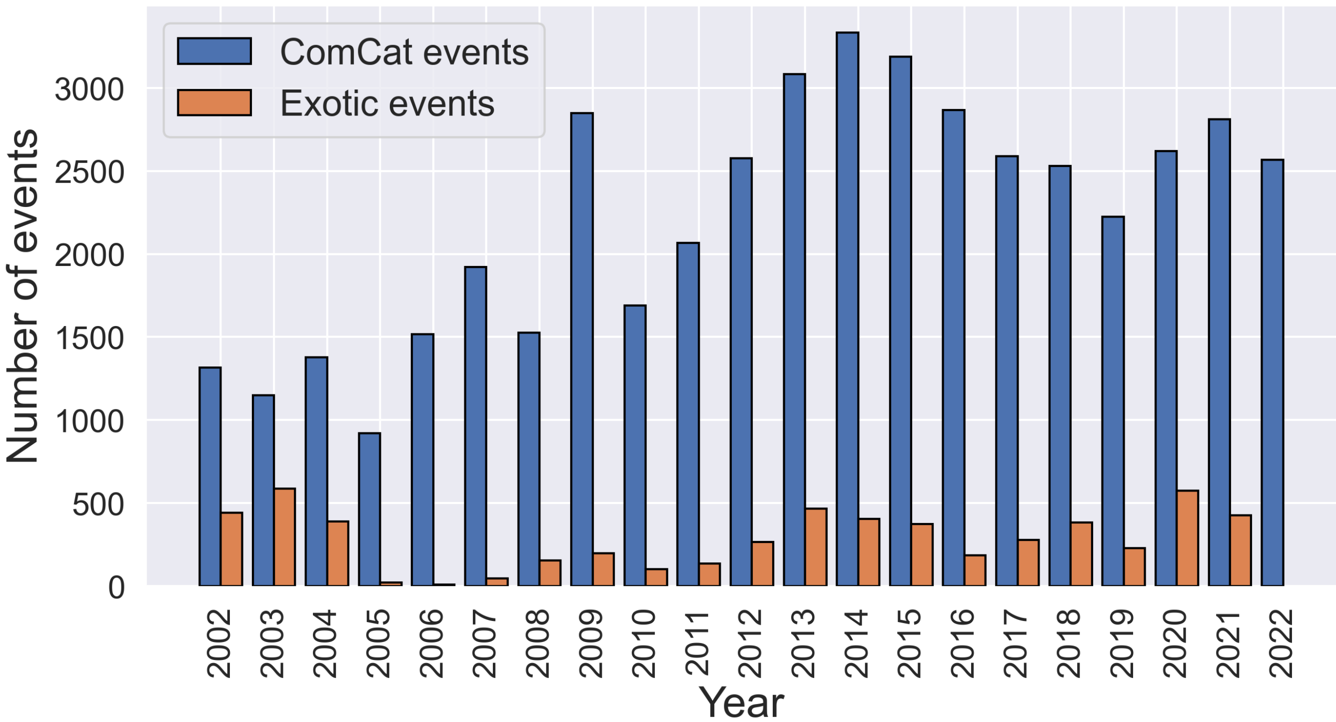

Figure 1 The event counts of ComCat and exotic catalog included in the AI-ready PNW data set as a function of time.

2.1.1 ComCat Events

We query the ANSS ComCat and download 65,384 events with magnitudes greater than 0 from 1 January 2002 to 31 December 2022, which we refer to as "ComCat events". We only select the events from ComCat sent by the PNSN, whose event ID has a "uw" prefix. The event metadata, including phase picks, are downloaded using libcomcat (Hearne and Schovanec, 2020) and stored in the QuakeML format (v1.2, Schorlemmer et al., 2011). The source type of these events are either earthquakes or explosions. The download contains 997,213 associated phase picks. Among these picks, 944,220 were made on velocity channels and only 52,982 (5.3%) on strong-motion channels. For single-channel stations where only the vertical channel (Z) exists (e.g., EHZ), S-waves were also picked only if the onsets were clear. The temporal evolution of the ComCat events reflects a combination of increased coverage and sensitivity of the seismometers. In 2009, a large number of the cataloged events came from an intense swarm of earthquakes at Wooded Island in eastern Washington (Gomberg et al., 2012). The number of events represented in our final curated data set is less than what we originally downloaded due to data selection criteria described in Section 2.3.

2.1.2 Exotic Events

We also collect data from 5,657 events cataloged by the PNSN since 2002 that are neither labeled as earthquakes nor explosions. The exotic events are not incorporated in the ANSS ComCat and are only available through the PNSN's ANSS Earthquake Monitoring System (AQMS) database. In this data set, we include events that were labeled as "surface event", "thunder", "sonic boom", and unfortunately a "plane crash" (a confirmed event near Whidbey Island, Washington, 3 March 2013). We refer to these events as "exotic events" herein. Figure 2 shows the number of events in each category for our final data set.

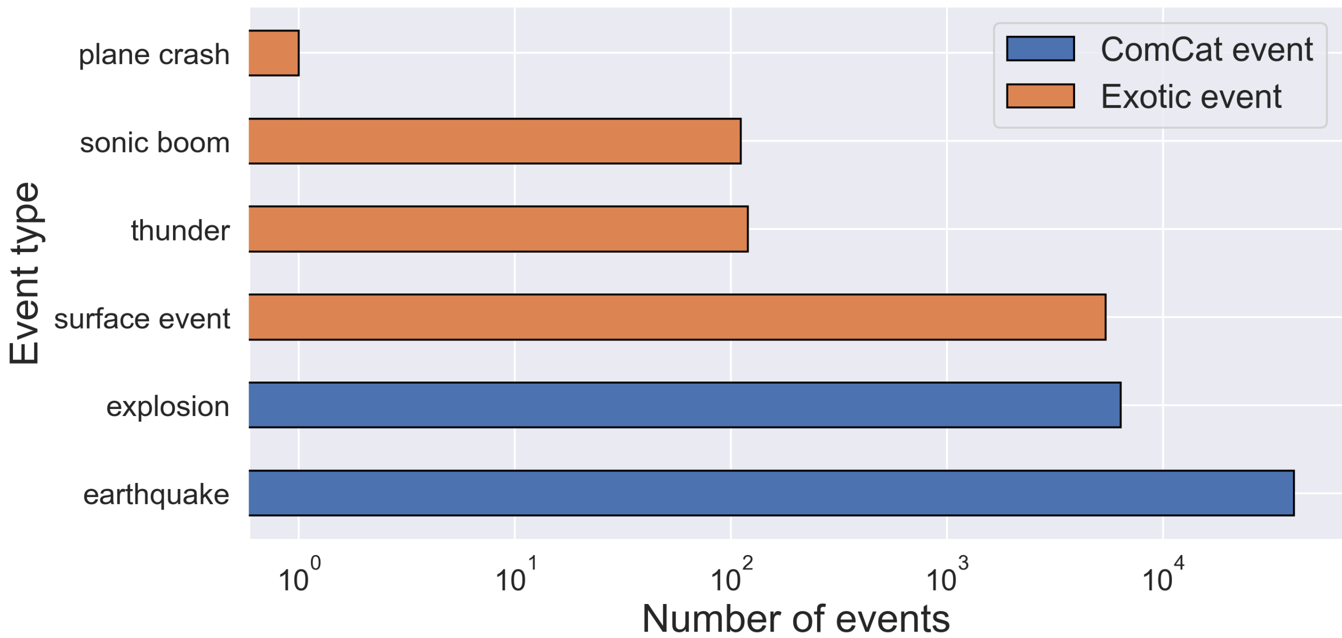

Figure 2 Number of events arranged by event type of the curated ComCat and Exotic event data sets.

The temporal evolution of the exotic event catalog depends on manual intervention by the analysts. Because non-tectonic earthquakes are not the priority of the PNSN, analysts only pick when time permits. Most of the labeled exotic events, such as surface events, are detected on well-instrumented volcanoes (see Figure S11). The lower event count in the period 2005-2008 coincides with volcanic unrest at Mt. St. Helens, when the network was also desensitized during this period to the events around Mt. St. Helens due to the intense rate of volcano-tectonic seismicity. It is quite possible that other surface events outside of the volcanoes are missing, due to having fewer stations elsewhere.

Most of the exotic events are small in magnitude and seismic amplitude and thus local to a few stations. Due to a lack of additional observation of the events (e.g., a ground truth imagery as done in the ESEC catalog), source characteristics such as the source origin time, location, and magnitude are not provided for these events.

2.1.3 2022 Northern California Ferndale Earthquake Sequence

We also include events associated with the 20 December 2022 M6.4 Ferndale (northern California) Earthquake. This sequence provided us with a rare opportunity to add labels for moderate-to-large earthquake sizes. These events are outside of the PNSN's authoritative boundary and, thus are not routinely processed by the network. We select 20 events of $M \geq 3$ reported by the California Integrated Seismic Network (CISN) from that sequence and manually pick 609 P-wave arrivals. Table S2 lists events included in the dataset.

2.2 Station Metadata

The station metadata describes the technical information necessary for seismic data processing and tracks the history of any metadata changes. The IRIS DMC stores station metadata as dataless SEED files, but they can be downloaded in the StationXML format from IRIS International Federation of Digital Seismograph Networks Web Service (FDSN-WS, `http://service.iris.edu/fdsnws`). The up-to-date station metadata we use is downloaded using ObsPy (Krischer et al., 2015). These stations are either long-term installations maintained by a seismic network (e.g., UW (University of Washington, 1963)) or long-time experiments that lasts several years (e.g., US Transportable Array, FDSN code TA (IRIS Transportable Array, 2003)).

2.3 Event Waveforms

All digitized data from the PNSN are requested and downloaded through the IRIS FDSN-WS (`http://service.iris.edu/fdsnws`). In total, we download ∼70 TB miniSEED from 1 January 2002 to 31 December 2022. We first curate waveforms from high-gain velocity seismometers, and specific channels from short-period (EH?) and broadband (either BH? or HH?) seismometers. We do not use the SL? and SH? channels since they are simply derived from EH? channel after low-pass filtering or down-sampling. We also include waveforms from strong-motion EN? stations separately since there are also picks made on these channels by the analysts. We do not correct for instrumental response and do not integrate the acceleration to velocity. All waveforms are resampled to 100 Hz from their original sampling rates, which may be 40 (most BH? channels) or 100 (most EH? and HH? channels). The resampling step is necessary for deep neural networks with fixed input sizes. We keep the data as is, even if it is clipped.

For each ComCat event, we only select the stations where both P- and S-wave are picked. We prepare 150-second data for ComCat events: the window starts 50 seconds before and ends 100 seconds after the source origin time (200 seconds after the origin time for the Northern California earthquake sequence). The same length of traces before this time window is curated as the noise waveforms. The reason for including so much noise window ahead of the origin time is to allow user flexibility when trimming and shifting the data in future investigations. In the ComCat events, less than 1% of the S-wave picks arrive later than 60 seconds after the origin time. Thus, most S-wave arrivals are included in the time window. Then, we apply a linear detrending. We also resample all waveforms to 100 Hz, which upsamples the board-band BH? channels. Due to the small inaccuracy (∼0.00008%) of the digitizer clock of the analog EHZ stations, the sampling rate at these stations shifts away from strictly 100 Hz. We correct this by resampling to 100 Hz. Gappy traces are discarded. Missing channels, for example, the vertical-component-only instruments (e.g., channel EHZ) are filled with zeroes to keep the consistency of a three-component stream (further detailed below). Picks are only done with data from a single instrument per site, even if a site may have several sensors. Therefore, each "stream" is independent of the other. Examples of earthquake waveforms can be found in Figure S19 and S20 for the velocity-seismograms and Figure S21 for the acceleration seismograms. Examples of explosion waveforms can be found in Figure S23 and S24.

The PNSN operates seismic stations that are particularly remote. The transfer of data through telemetry sometimes leads to artifacts in the time series. Furthermore, the transition from triggered to continuous data was progressive, and sometimes, both triggered waveforms, which are detrended, and continuous data, unprocessed, are sent together: the triggered data overwrites the continuous data, creating a step in the data. These show in both short-period (EH?) and board-band (BH? and HH?) stations. For example, the time series may contain offsets that could be corrected in the future in the seismic archive at the IRIS DMC (see Figure S4).

The waveforms extracted for an exotic event are not aligned with the source origin time, which is mostly unknown. Instead, we align the waveforms by the phase picks that were provided by the analysts. The waveforms start 70 seconds before P-wave picks or 80 seconds before S-wave picks, whichever is available. Most exotic events have no picked S-waves, but if both P- and S-wave picks exist, the P-wave is prioritized to align the time window. The time window is 180 seconds long for all types of exotic events, given the occasional long duration and elongation (e.g., cigar-shaped waveforms (Manconi et al., 2017)) of the surface events. We follow the same data-curating process and formats as we process the ComCat events. Examples of surface-event waveforms can be found in Figure S25 and S26. Examples of thunderquakes can be found in Figure S28 and S27. Examples of sonic boom events are found in Figures S30 and S29, and all waveforms from the plane crash event in Figure S31.

We also extract noise-only waveforms. These waveforms are extracted just ahead of the event waveforms. We selected high-gain velocity channels (EH?, HH?, and BH?) using a random selection. To further test if there are hidden events in the noise waveforms, we run the machine learning model (see Section 2.4) to test whether events could be detected and only found very few occasions where events may have been present.

We organize the three-component waveforms into NumPy arrays and define a *stream* as a three-component array (Harris et al., 2020; Krischer et al., 2015). To improve accessibility in the machine-learning ecosystem, we follow the SeisBench data format convention. The metadata is stored in CSV (comma-separated values) files, while all waveforms are stored in the Hierarchical Data Format version 5 (HDF5) format. The signal-to-noise ratios (SNR) are calculated (detailed below) and saved as attributes in the metadata file.

After applying the selection criteria described above, more than 70% of the ComCat events are kept in the data set. Figure 3 shows the map of the selected events. The data sets cover events within the authoritative boundary of the PNSN, offshore in the Jan de Fuca Ridge, underneath Vancouver Island, and further East in Idaho. We provide an overview of the final number of ComCat waveforms and events in Table 1. The summary compiles the data volume across magnitudes from 0 to 6.4. It is possible that most of the events discarded by the selection had no S-wave picks for clipped waveforms. Our selection criteria also excluded more events before 2010, which we attribute to the much fewer S picks available when the data is clipped or when only vertical-component stations are available.

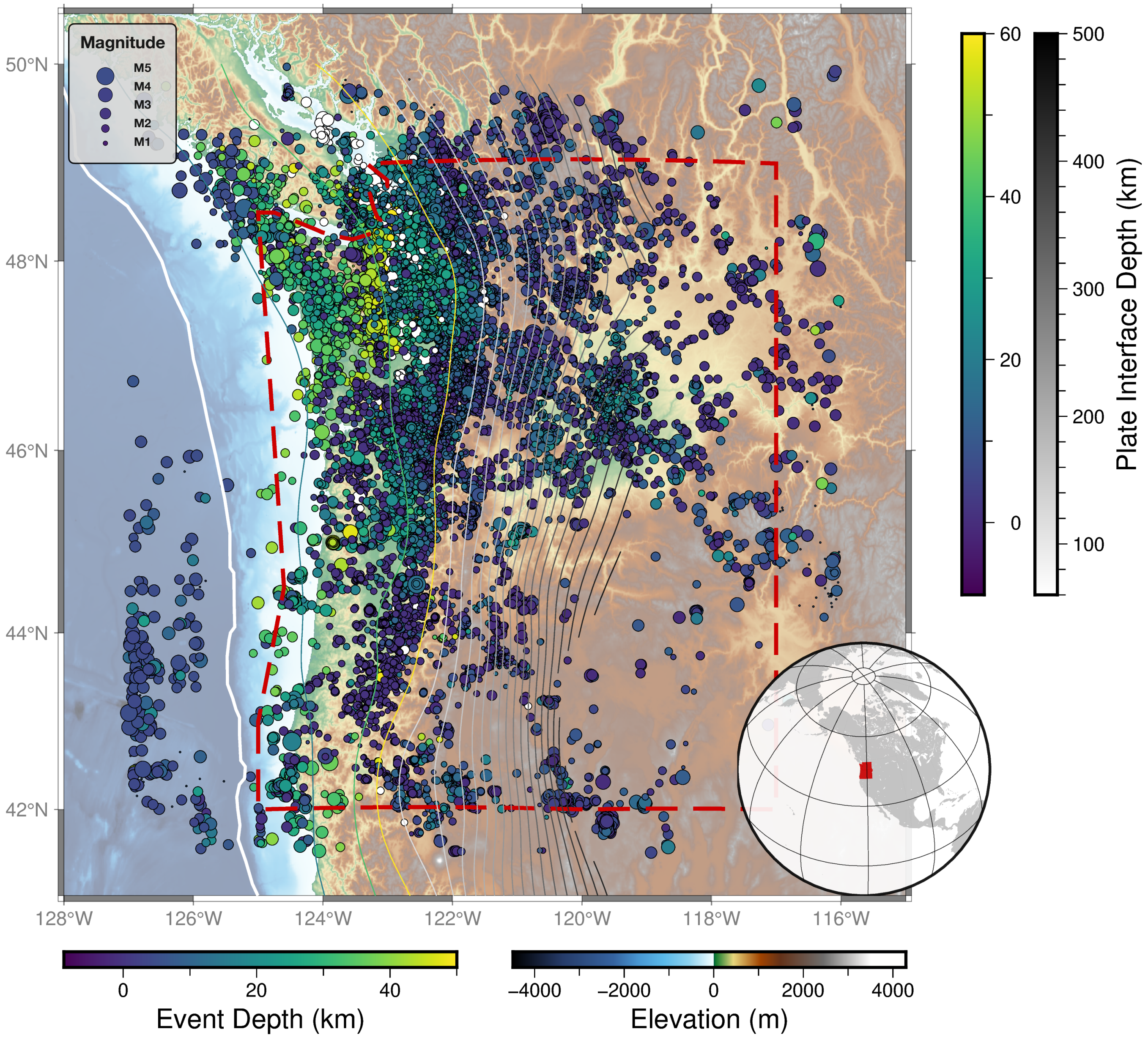

Figure 3 Locations of the events included in the ComCat data set. The red dashed polygon denotes the authoritative region boundaries of PNSN. The solid lines mark the depth contour of the subduction slab with a 20 km interval Hayes (2018). The plate boundary between Juan de Fuca and North America Plate (plate depth 0 km) is delineated in the white line. Some events are color-coded white because they are deeper than 50 km. These are intermediate-depth earthquakes.

2.4 Machine Learning Phase Picker and Enhanced Earthquake Picks

We provide an alternative catalog of phase picks from the earthquake event catalog as a use-case of the data set and a research-grade catalog of new picks of P and S waves using Machine Learning (ML). Automating phase picking using deep neural networks has revived the methodological development for picking seismic waves (Mousavi and Beroza, 2022; Münchmeyer et al., 2022).

Here, we use the Earthquake Transformer architecture from Mousavi et al. (2020) and implement phase-picking benchmark tests on the ComCat events. The SeisBench toolbox provides a set of Earthquake Transformer weights for models pre-trained with different data sets. We select all windowed waveforms from HH?, BH? and EH? channels and detrend the waveform. We compare the picks made by these models trained on STEAD, ETHZ, SCEDC, and INSTANCE data sets with the PNSN analyst picks recorded in the ComCat events. We demonstrate their performance by showing

Magnitude range	Number of included events	Percentage of available events	Number of independent streams
0 - 1	19,735	77.1%	70,168
1 - 2	21,717	79.2%	95,406
2 - 3	4,825	42.8%	21,901
3 - 4	398(15)	37.9%	2,332
4 - 5	31(3)	77.5%	205
5 - 6	1(1)	100.0%	4
6 - 7	0(1)	N/A	0
0 - 7	**46,707**	**71.4%**	**190,016**

Table 1 Number of included ComCat events as a function of event magnitude. The magnitude used here includes duration (Md) and local (Ml) magnitude. The number of streams includes both velocity and acceleration channels. Also provided is the number of included events as a percentage of downloaded ComCat events. Numbers in the parentheses show the events from the 20 December 2022 Northern California earthquake sequence.

the residuals between ComCat picks, and ML-predicted picks for P- and S-waves. The performance metrics are the mean absolute error (MAE), the root-mean-square error (RMS) for the phase picking, and the percentage of detected picks relative to ground truth picks.

The input size of the Earthquake Transformer using SeisBench is 3-component, 60 seconds at 100 Hz. The probability threshold for picking is 10%. Figure 4 shows the distributions of the residuals among models and for both P and S wave picks.

The approaches to benchmark the detection and picking performance are i) the seismic network-specific expectations for the manual picking uncertainties and ii) the comparison of bias and variance in the residual distributions relative to other studies (Mousavi et al., 2020; Münchmeyer et al., 2022). We find a general trade-off between detection accuracy (completeness) and phase-pick quality (low errors). The model trained with the STEAD data set has the best picking accuracy, but it misses more than 20% of the detections. In contrast, the model trained with the SCEDC data set had the best detectability and only missed about 5% of arrivals for both P- and S-waves, but the picking accuracy, especially that of S-waves, is poor. There is also a similar pattern on the model trained with ETHZ and INSTANCE data set in Figure 4. The performance trade-off between detection and picking accuracy makes retraining the phase pickers using the PNW data necessary.

Using our curated data set of ComCat earthquakes and explosions, we retrain the Earthquake Transformer model. Instead of training from scratch (randomly initialized weights), we start the training from the SeisBench-trained model, which used the STEAD data set, and continue training for additional 100 epochs on our data set. We use a small learning rate (1×10^{-4}) with Adam optimizer (Kingma and Ba, 2014) during the training. Compared with the other pre-trained models, the transfer-learning on the PNW data set improves the detection accuracy, considerably improves the S-wave picks, and gives as good of a performance as the STEAD-trained data set (see Figure 4). We also test all these models on strong-motion (acceleration) channels, for which INSTANCE contains the most acceleration waveforms (28.3%). The PNW transfer-learned model outperforms other pre-trained models, as shown in Figure S1.

The ability to find more and accurate picks by the retrained Earthquake Transformer makes it possible to create a future Machine-Learning-enhanced earthquake catalog. We revisit waveforms from the ComCat events that included either P or S picks. There are 683,133 P- and 244,431 S-wave picks for 62,054 events from these waveforms. We detect 16,201 (2%) and 207,146 (85%) new arrivals out of 686,748 time windows for P- and S-waves using the refined phase picker. As a crude quality control, we remove the picks where the ratio between the S-travel time and the P-wave travel time exceeds 2.5 or below 1.5. We add these picks with PNSN manual picks as a part of the curated data set in a separate file. We also use this retrained model to predict the noise waveform and drop those with any prediction greater than 0.1. This step effectively removes unpicked seismic events in the noise waveform.

3 Description of the AI-ready Data Set

The data sets consist of two files per set, one HDF5 file containing the waveforms and a CSV file with the metadata (attributes).

3.1 Waveforms

There are 190,016 and 9,267 three-component streams curated from ComCat and exotic event catalogs, respectively. Figure 5 shows the counts of streams arranged by channel type as a yearly estimate. We store all waveforms in HDF5 files using h5py (Collette et al., 2021) and index them by the trace name in the metadata. The attribute `trace_start_time` in `YYYY-MM-DDTHH:MM:SS.SSSZ` format describes the UTC time at which the stream begins. A code block 1 illustrates how users can read the waveform data and locate the stream in Python.

Listing 1 Read stream data from SeisBench format waveform file using h5py

```
import h5py
```

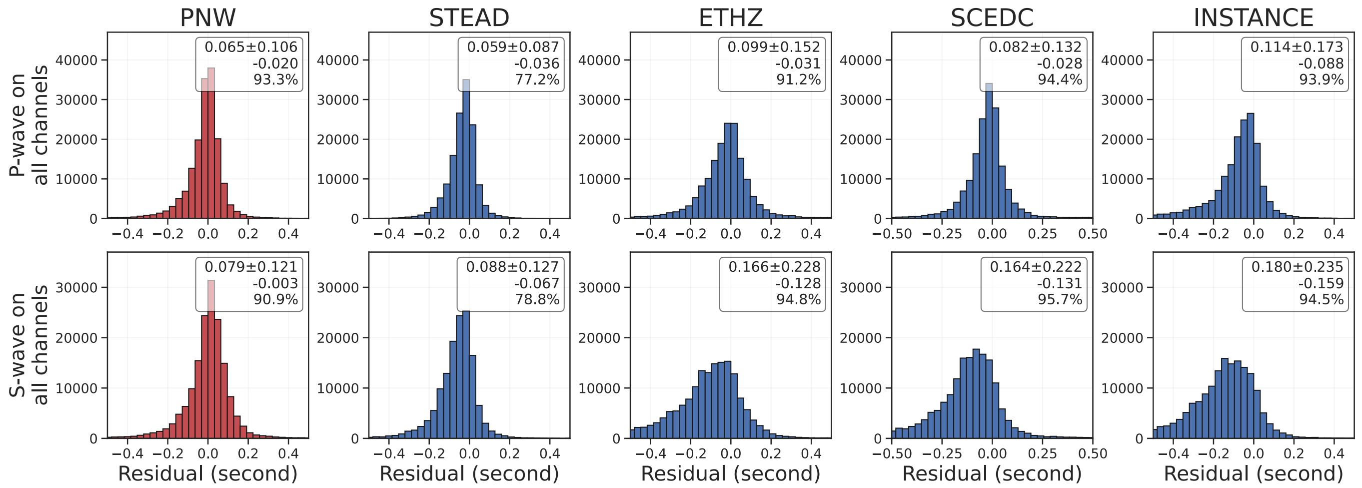

Figure 4 Distributions of P- and S-wave picking residuals ($t_{ML} - t_{PNSN}$) from the benchmark testing on velocity seismograms. The number in the upper right corner of each subplot shows the mean absolute error (MAE), the root-mean-square error (RMSE), the mean value of the residual, and the picking completeness in percentage concerning the ground truth. The PNW-retrained Earthquake Transformer outperforms the other four pre-trained models from SeisBench (Woollam et al., 2022) in both picking accuracy and detecting completeness.

```
f = h5py.File("/path/to/waveform.hdf5", "r")
trace_name = "bucket1$0,:3,:15001"
bucket, array = trace_name.split('$')
x, y, z = iter([int(i) for i in array.split(',:')])
data = f[f'/data/{bucket}'][x, :y, :z]
```

The data is saved as vertical concatenated NumPy arrays of fixed window length (here 150 s), three components. It is distributed over several "buckets" that are "groups" under the HDF5 taxonomy. The trace name (a data attribute saved in the metadata dataframe), the index of the data in the bucket, and the index of the first dimension.

3.2 Metadata

The metadata describes the waveform data and its attributes and is essential to our data set. Each stream corresponds to one record (or a row) in the metadata file. We follow SeisBench conventions again. The unit of each attribute is appended as part of the attribute's name. For example, `source_latitude_deg` indicates the latitude of the source in degrees. A full description of the attributes is listed in Table 2. As many attributes are self-explanatory, we provide more details below.

3.2.1 Station network code

Stations selected in both data sets may come from nine different FDSN network codes. These stations are either installed and maintained by PNSN (e.g., UW and UO) or used by PNSN when doing phase picking and events locating (e.g., PB, CC, IU, CN, HW, TA, US). Maps of the stations shown in the data set show a similar distribution for both ComCat (Figure S10) and exotic events (Figure S11). All stations are in-land stations, and no off-shore stations (e.g., OOI) are used in our dataset. The numbers of streams from each FDSN network and their references are listed in Table 3. PNSN stations contribute more than 85% of streams in the ComCat and Exotic event data sets.

3.2.2 Event ID

An event identifier (ID) is given to each event by the PNSN after the processing is finalized and sent to ANSS through USGS Product Distribution Layer (PDL). The ComCat events contributed by the PNSN have IDs of eight-digit numbers with a "uw" prefix, e.g., "uw10568488". The event IDs are unique in the catalog. The exotic event IDs are internal to the PNSN AQMS database and cannot be accessed through USGS. To distinguish them from ComCat events, we add a "pnsn" prefix to their event IDs.

3.2.3 Event Type

When processing a seismic event as the seismic data comes in, the event type is manually specified by the network analysts. For example, the PNSN labels "probable explosion" waveforms that have the characteristics of shallow quarry blasts (strong P waves and location near known quarries). Until the 1990s, the PNSN would confirm these explosions by phone confirmation, though this is no longer routinely done. When sending the finalized event from the AQMS database to the ComCat, PNSN maps and merges several types of events into one: "earthquake", "slow earthquake",

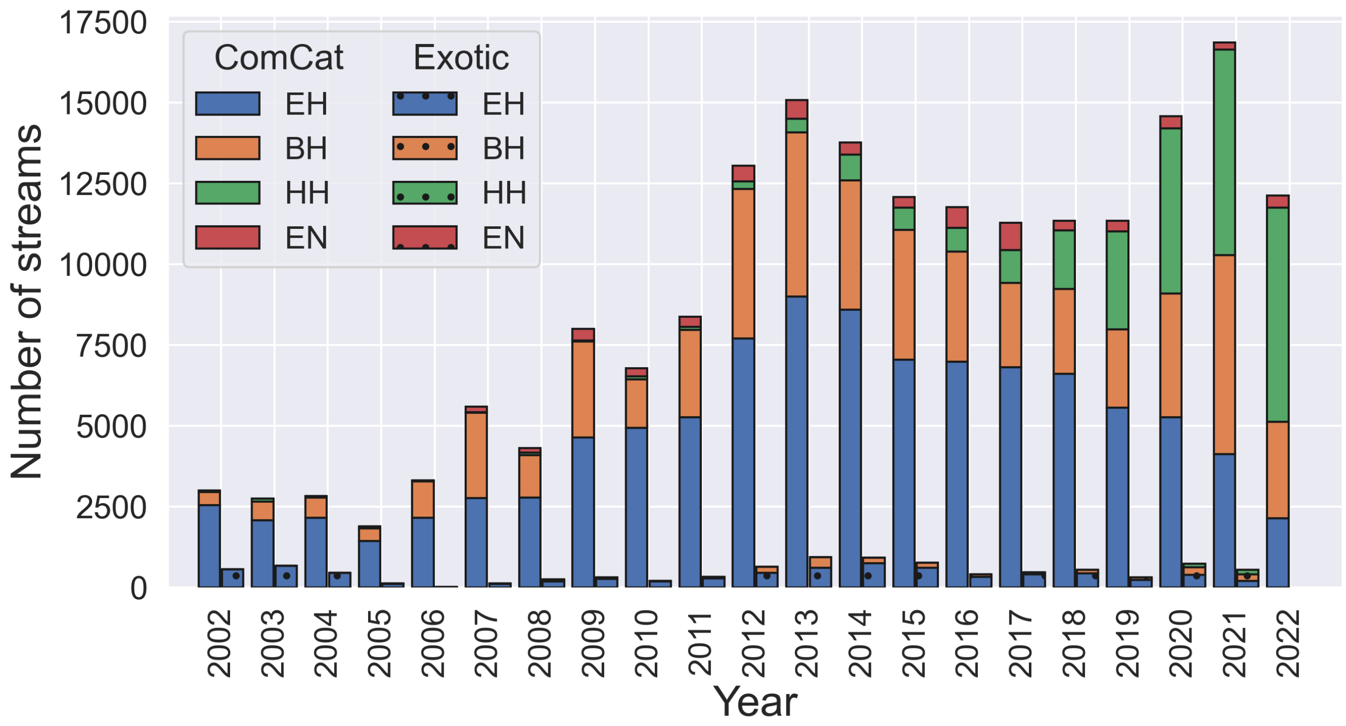

Figure 5 Number of streams from each channel type used in the ComCat and exotic event catalogs through time. Short-period (EH?) and board-band (BH?) sensors were the predominant channels for both ComCat and exotic data sets before 2012, while the recording at higher sampling rates at broadband sensors (HH?) increasingly has become the standard since then. A limited number of streams from strong-motion accelerometer EN? channels is available in the data set since 2007.

and "long period volcanic earthquake" are mapped into the "earthquake" category; "explosion", "shot" and "probable explosion" are merged into the "explosion" category. For simplicity and consistency, we use the event types "earthquake" and "explosion" for the ComCat events, but their original event types are also included for reference in the metadata. Table S1 lists the latest PNSN event-type labels from the PNSN AQMS database.

3.2.4 Source Magnitude and Type

The event size, as represented by the source magnitude, is only available for the ComCat events. All ComCat events included in the data set have magnitudes less than seven and greater than zero, as shown in Table 1. The magnitude completeness of the catalog is estimated using the method of Wiemer and Wyss (2000) and found to be around 2 for the years 2019-2022 (see Figure S9). The types of magnitudes reported are typical to regional earthquakes that have local seismicity: the local magnitude (Ml) and the duration magnitude (Md).

There are three types of magnitude used in the data set. The PNSN uses a local magnitude (Ml) (Richter, 1958; Jennings and Kanamori, 1983) that measures the magnitude of a local earthquake using the average maximum amplitudes of two horizontal seismograms converted to have the Wood-Anderson response, preferably taken from broadband seismometers, and corrected for the distance between the source and the receiver. Such magnitude is reported by the National Earthquake Information Center (NEIC) for all earthquakes in the US and Canada. The coda duration magnitude Md is calculated based on the duration of shaking measured on the vertical component and could be the only available magnitude product for small events or those not well recorded on well-calibrated stations with horizontal components. Over the course of time, processes to calculate the magnitudes vary because of varied processing routines and analyst interventions.

Until 2012, the PNSN only reported duration magnitude to ComCat for most earthquakes using the algorithm from Crosson (1972), except for a few significant events that were manually changed to the local magnitude. The early seismic stations of the PNSN only had vertical components, a small dynamic range, and short-period sensors that would clip even for relatively small magnitude events. It is not possible to obtain a local magnitude from such data. As the network modernized over time, higher dynamic-range three-component sensors were added, the data quality improved, which allowed PNSN to determine an Ml for more events. From 2002 to 2011, 46,326 events had duration magnitude preferred, while only 483 events (average magnitude 2.45) had local magnitude reported as the preferred magnitude type. From 2012 to 2015, the PNSN calculated and reported both duration and local magnitudes, though the local magnitude was still only calculated for larger events. Since 2015, the PNSN has switched from having duration magnitude to the local magnitude as the preferred and default magnitude. 80% of all events included in the ComCat data set until 2008 have a duration magnitude preferred, after when there were increasingly more Ml-

Attribute	Description	Example
event_id	Event identifier	uw10564613
source_origin_time	Source origin time in UTC	2002-10-03T01:56:49.530000
source_latitude_deg	Source latitude in degree	48.553
source_longitude_deg	Source longitude in degree	-122.52
source_type	-	earthquake
source_type_pnsn_label	PNSN AQMS event type	eq
source_depth_km	Source latitude in kilometer	14.907
source_magnitude_preferred	-	2.1
source_magnitude_type_preferred	-	Md
source_magnitude_uncertainty_preferred	-	0.03
source_local/duration/hand_magnitude	Ml, Md, and Mh if available	1.32
source_local/duration_magnitude_uncertainty	Magnitude uncertainty if available	0.15
source_depth_uncertainty_km	Source depth uncertainty in kilometer	1.69
source_horizontal_uncertainty_km	Source horizontal uncertainty in kilometer	0.694
station_network_code	FDSN network code	UW
station_code	FDSN station code	GNW
station_location_code	FDSN location code	01
station_latitude_deg	Station latitude in degree	47.5641
station_longitude_deg	Station longitude in degree	-122.825
station_elevation_m	Station elevation in meter	220.0
trace_channel	FDSN channel code (first two digits)	BH
trace_name	Bucket and array index	bucket1$0,:3:15001
trace_sampling_rate_hz	All traces resampled to 100 Hz	100
trace_start_time	Trace start time in UTC	2002-10-03T01:55:59.530000Z
trace_P/S_arrival_sample	Closest sample index of arrival	8097
trace_P/S_arrival_uncertainty_s	Picking uncertainty in second	0.02
trace_P/S_onset	P- or S-wave onset	emergent
trace_P_polarity	P-wave arrival polarity	positive
trace_snr_db	SNR for each component	6.135|3.065|11.766

Table 2 Attributes in the metadata file. Some source attributes are not available for exotic events.

preferred magnitudes (Figure 6). While the duration magnitude is still calculated, it is only the preferred magnitude for about 10% of the events each year. From 2002 to 2022, there were also 111 events with an Mh magnitude in the data set, extracted from the NEIC and manually added by the network analysts. Note that there is no moment magnitude Mw reported in this data set because the moment magnitude is obtained from low-frequency seismograms, which are often buried in the seismic noise for small earthquakes. Mw magnitude may be included as Mh.

There are potential challenges in interpreting the magnitudes as ground truth labels. Md and Ml have known systematic biases that arise from the particularly high near-source scattering of shallow earthquakes or quarry blasts (Koper et al., 2020; Wang et al., 2021). In 2012, the PNSN adopted AQMS, which included a method to measure coda duration that was not consistent with the previously used method. The PNSN staff did a rough recalibration of their Md relationship to partially account for the systematic difference. However, there is a known inconsistency of the Md magnitudes for the smallest events before 2012 and after 2012. Future efforts must be made to re-calculate the magnitudes more systematically, ideally using consistent methods, throughout the 2002-2022 period.

Table 1 shows the event counts per magnitude bin for this data set. The largest event in the data set comes from Mw 6.4 Northern California, 20 December 2022 by the CISN, but this event was outside the PNSN's authoritative boundaries. Thus, ComCat preferred an origin contributed by CISN. The largest earthquake in this data set within PNSN's authoritative boundaries is Md 4.8 Brinnon, Washington, on 25 April 2003 (event ID uw10583988). Relatively small magnitude uncertainty (0.04), depth uncertainty (0.59 km), and horizontal uncertainty (0.347 km) were reported.

3.2.5 Stream Signal-to-Noise Ratio

The signal-to-noise ratio (SNR) is an important factor in measuring the noise level in the traces. Similar to Michelini et al. (2021), we define the noise window as 8 seconds before the P-wave arrival for the ComCat events. To better capture the energy of emergent S-wave onsets, the signal window is defined as 1 second before to 2 seconds after the S-wave arrival. For the exotic event catalog, since P-wave and S-wave arrivals may not be available, the noise window is defined to begin 12 seconds after the beginning of the traces. The signal window is the same as exotic events, P- or S-wave, whichever is available. For each component, the SNR is defined as

$$SNR = 20 \log_{10} \frac{|S_{98}|}{|N_{98}|} \tag{1}$$

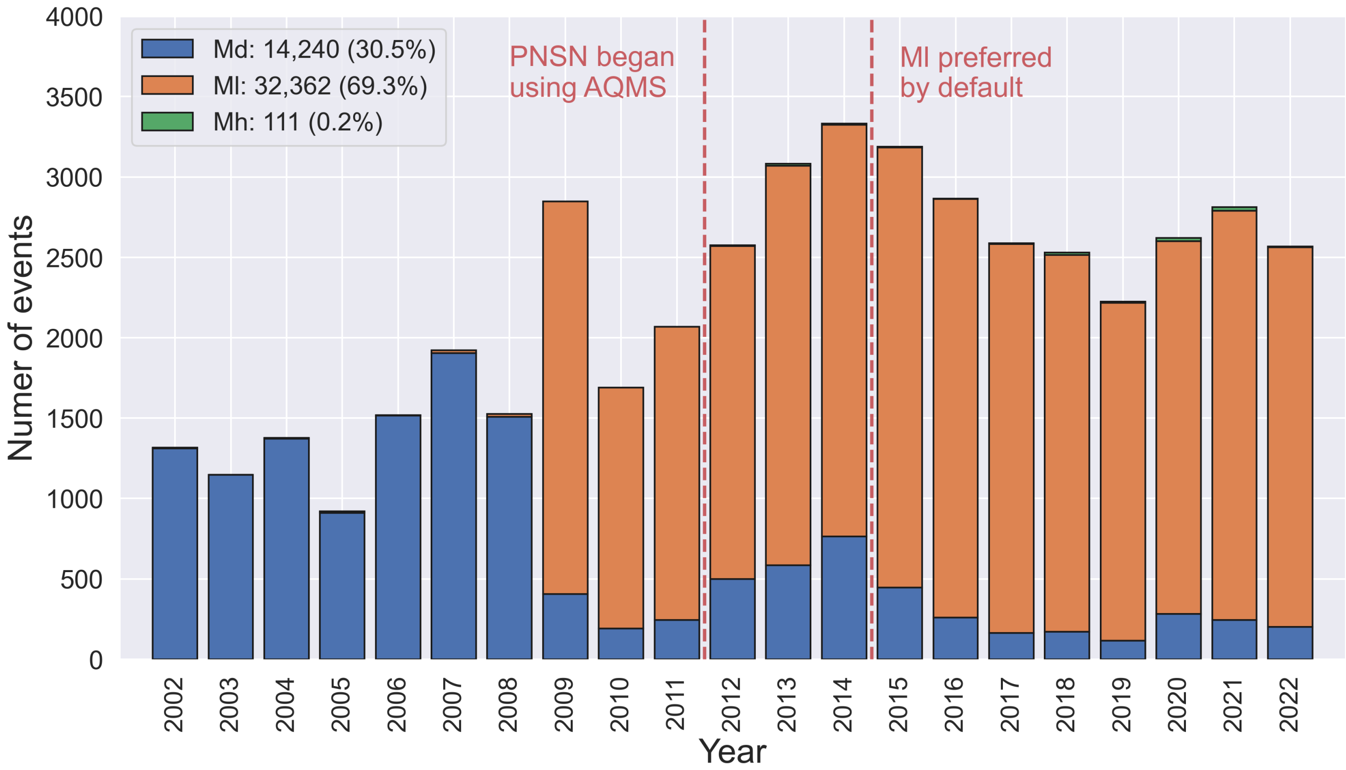

Figure 6 Magnitude types of ComCat events as a function of time. Md and Ml denote duration and local magnitudes, respectively. Mh denotes magnitudes manually inserted by the analysts. Before the PNSN began using the ANSS Earthquake Monitoring System (AQMS) in 2012, 483 events had Ml estimates, and 46,326 events had Md estimates in the data set.

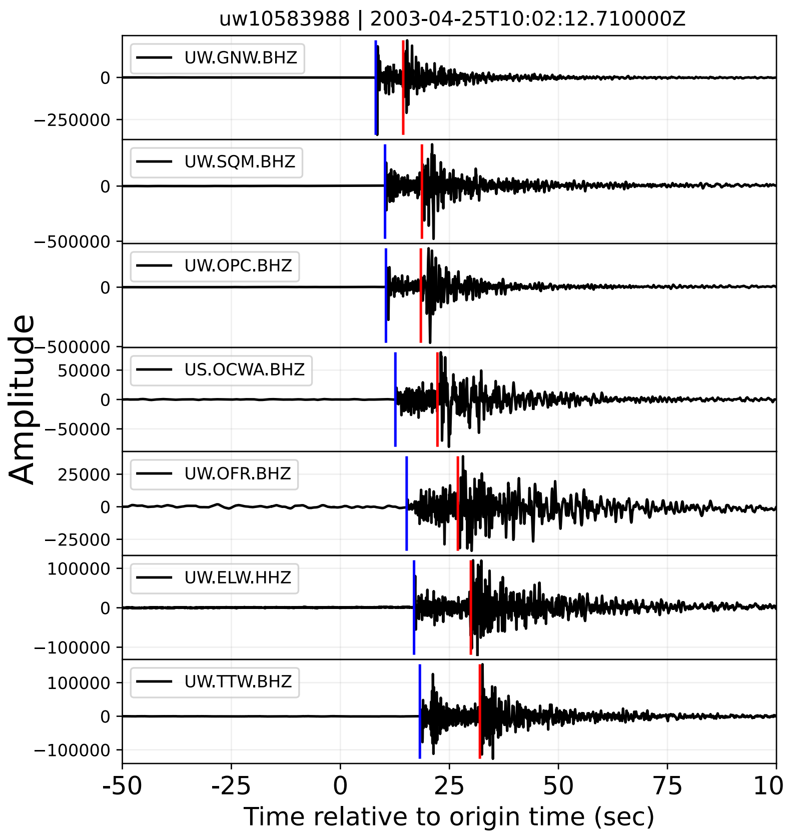

Figure 7 Waveform from event uw10583988 (M4.8 Brinnon, Washington, 25 April 2003) included in the data set. Only the vertical component is shown. The blue and red vertical lines show P- and S-wave arrival picked, respectively.

where $|S_{98}|$ and $|N_{98}|$ are the 98% percentile of the absolute values in the signal and noise window, respectively. When no data is available, e.g., a single-channel station with only the EHZ channel, **NaN (not-a-number)** is filled as a placeholder in the missing channels. Figure 8 shows the distribution of individual SNRs calculated from the ComCat and exotic event catalogs. The traces with SNR $> 80\ db$ (indicating an error in the noise window) or $< -20\ db$ (indicated too low of a signal) are removed from the data set.

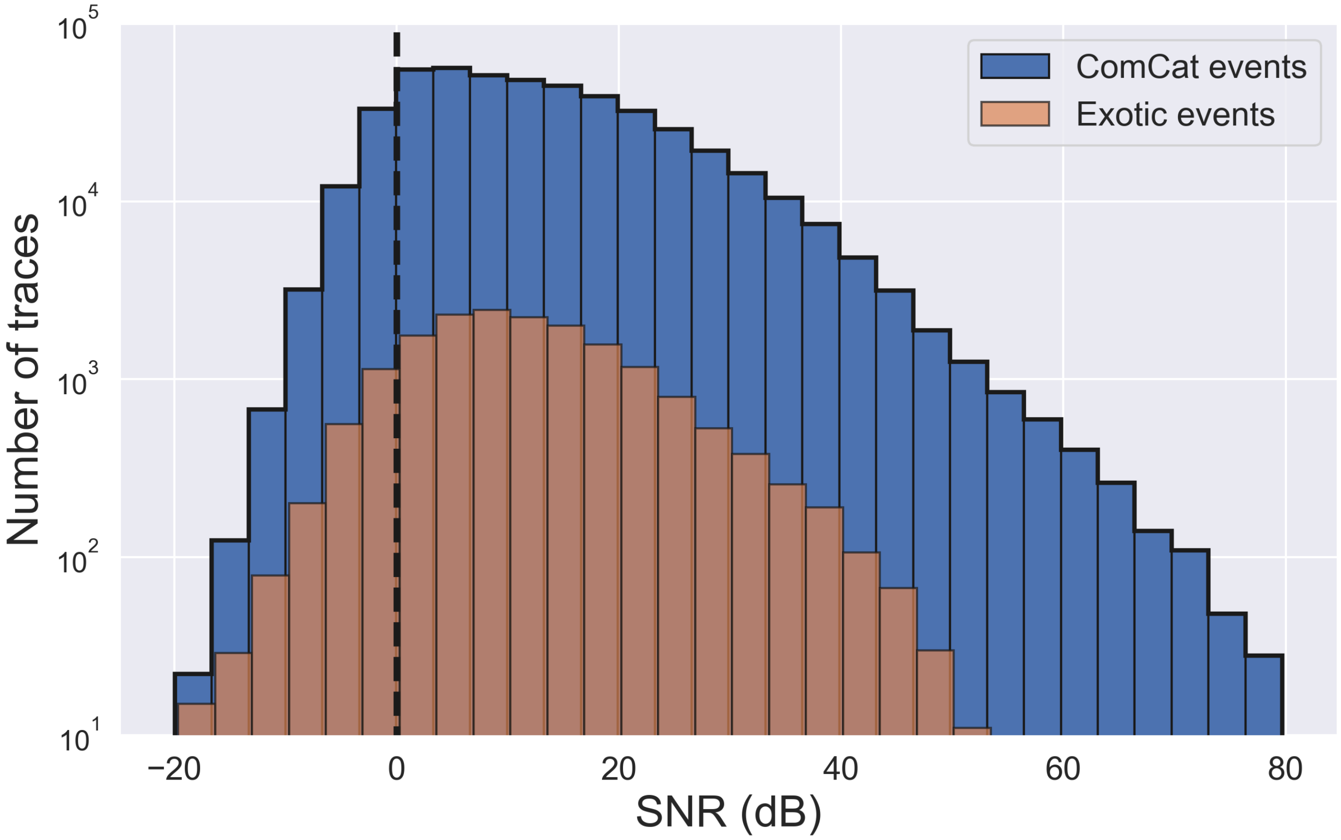

Figure 8 Distribution of signal-to-noise ratios (SNR) of the traces from ComCat and exotic events. SNRs are calculated on each component of the three-component streams.

3.2.6 Uncertainties

The metadata includes four types of uncertainties for the ComCat events. The P- and S-waves arrival uncertainties are estimated at the time of picking. Before the PNSN used AQMS, the uncertainty was directly measured and recorded in the phase data, and a weight was calculated. Using Jiggle from AQMS since 2012, the analysts assign weight as an integer ranging from zero to four to each pick by visually measuring the impulsivity of the arrival. A zero weight indicates the highest accuracy of picks, typically for P-wave arrivals, and has 0.03 seconds of uncertainty. A weight of three indicates a low pick accuracy, typically for S-wave arrival with 0.3 seconds of uncertainty. Phase uncertainties are used when locating the events, but those with uncertainty weights of four are typically not used in earthquake locations. Before 2012, PNSN used Spong (an adaption of Fasthypo (Herrmann, 1979)) as the location engine. This changed to HYPOINVERSE (Klein, 2002) after PNSN started using AQMS and Jiggle.

The origin location (depth and horizontal) uncertainties are the error estimated from the location engine. Figure S13 shows the locations of the events with horizontal uncertainty greater than 20 km. Note the cluster off-shore Oregon that is outside of the PNSN authoritative boundaries. The PNSN has poor location constraints on these events since there are almost no offshore seismic stations except for the Ocean Observatories Initiative Regional Cable Array (FDSN network code OO (Rutgers University, 2013)), which are occasionally picked during PNSN routine data processing. ComCat may not choose these origin products from PNSN as preferred. However, the events with high horizontal uncertainty only make up 0.4% of all ComCat events, and their picks are still accurate enough to be part of the data set.

We also include the magnitude uncertainties in the metadata. The magnitude is first evaluated on the channel level. For three-component stations, the channel-level local magnitude is calculated only if a P- or S-wave is picked on one of the components to only select clear signals. Since 2012, a few single-component stations (EHZ) also contribute to the local magnitude and have the same weight as three-component stations. The event magnitude is the median of all channel magnitudes that meet the SNR criteria. The event magnitude uncertainty is the median absolute deviation (MAD) of channel magnitudes used for event magnitude calculation. These uncertainties are calculated for all magnitude types except Mh.

3.2.7 P-wave Polarity

When analysts pick the phase arrivals, Jiggle also automatically measures the first motion of the P-wave picks with weights less than one (e.g., best waveforms), leaving the rests as "undecidable". The analysts can manually override these polarities if they are confident. Less than 42% of P-waves in this data set have undecidable polarity information. The P-wave polarity ratio between positive and negative as a function of the year is shown in Figure S8. The sudden switch to a preference to assign or report positive polarities in 2012 highly suggests that the switch to AQMS and Jiggle in 2012 has affected the PNSN analysts' output. Until this data collection effort, we were unaware of this fact, and the reason for the abrupt change is unclear.

Network FDSN Code	Number of Streams	Reference
UW*	100,561|5,653|26,716	University of Washington (1963)
PB	41,674|461|11,126	Plate Boundary Observatory Borehole Seismic Network
CC	23,988 | 3,119 | 6,784	Cascades Volcano Observatory/USGS (2001)
TA	9,912 | 4 | 3,012	IRIS Transportable Array (2003)
CN	6,008 | 2 | 1,692	Natural Resources Canada (NRCAN Canada) (1975)
US	3,420 | 0 | 981	Albuquerque Seismological Laboratory (ASL)/USGS (1990)
UO*	3,593 | 28 | 891	University of Oregon (1990)
HW	840 | 0 | 252	Hanford Washington Seismic Network
IU	20 | 0 | 4	Albuquerque Seismological Laboratory (ASL)/USGS (1988)

Table 3 Description of network FDSN code and their references. Networks annotated by an asterisk mark (*) are maintained by the PNSN. The number of streams shown for each network is from ComCat events, exotic events, and noise, respectively. PB and HW network does not have a registered FDSN network DOI.

4 Conclusion

This work contributes to collecting and curating a seismic data set for the Pacific Northwest region. The curated data set is provided with the long-standing work and labeling of the Pacific Northwest Seismic Network analysts and seismologists. We described the temporal and spatial characteristics of the data attributes.

This original contribution focused on preparing the seismic waveforms and PNSN-provided data attributes (phase picks and default source parameters). We picked additional waveforms for the recent 20 December 2022 Northern California earthquake sequence, the largest event recorded recently in proximity to the PNSN authoritative boundaries. We also transfer-learned an established phase picker, the Earthquake Transformer (Mousavi et al., 2020), on the best quality of the PNSN picks and provided additional picks for S waves, which we provided in this contribution as an alternate catalog of picks.

There remains tremendous work to improve the quality and consistency of the data attributes. In particular, the attribute "magnitude" should be carefully interpreted as 60% of the catalog uses duration magnitude, and 40% of the catalog uses the local magnitude, but both may have biases. Therefore, a follow-up task is to re-calculate these magnitudes using consistent methods. Another avenue for improvement is to re-estimate the polarity of the P and S waves, using the known labels and predicting the "undecided" labels. An obvious next step will be event classification work that will take the waveforms and predict the event type.

Acknowledgements

Funding was provided by the PNSN (USGS cooperative agreement G20AC00035), the NSF SCOPED award (EAR 2103701), and a fellowship to MD by the David and Lucile Packard Foundation.

Code and Data Availability

The facilities of IRIS Data Services, and specifically the IRIS Data Management Center, were used for access to waveforms, related metadata, and derived products used in this study. IRIS Data Services are funded through the Seismological Facilities for the Advancement of Geoscience (SAGE) Award of the National Science Foundation under Cooperative Support Agreement EAR-1851048. The earthquake catalog on ComCat contributed by PNSN was downloaded using libcomcat (Hearne and Schovanec, 2020). The Earthquake Transformer implementation is from SeisBench toolbox (Woollam et al., 2022). All plots are made with Matplotlib (Hunter, 2007) and PyGMT (Uieda et al., 2021). The final data sets and the codes used in this study are available at `https://github.com/niyiyu/PNW-ML` (Ni, 2023).

References

A.A.Royer and M.G.Bostock. A comparative study of low frequency earthquake templates in northern cascadia. *Earth and Planetary Science Letters*, 402:247–256, 2014. doi: 10.1016/j.epsl.2013.08.040.

Albuquerque Seismological Laboratory (ASL)/USGS. Global seismograph network - iris/usgs, 1988.

Albuquerque Seismological Laboratory (ASL)/USGS. United states national seismic network, 1990.

Allen, R. Automatic phase pickers: Their present use and future prospects. *Bulletin of the Seismological Society of America*, 72(6B):S225–S242, 1982. doi: 10.1785/BSSA07206B0225.

Allstadt, K. Extracting source characteristics and dynamics of the august 2010 mount meager landslide from broadband seismograms. *Journal of Geophysical Research: Earth Surface*, 118(3):1472–1490, 2013. doi: https://doi.org/10.1002/jgrf.20110.

Allstadt, K., McVey, B., and Malone, S. Seismogenic landslides, debris flows, and outburst floods in the western united states and canada from 1977 to 2017: Us geological survey data release, 2017.

Allstadt, K. E., Matoza, R. S., Lockhart, A. B., Moran, S. C., Caplan-Auerbach, J., Haney, M. M., Thelen, W. A., and Malone, S. D. Seismic and acoustic signatures of surficial mass movements at volcanoes. *Journal of Volcanology and Geothermal Research*, 364:76–106, 2018a. doi: https://doi.org/10.1016/j.jvolgeores.2018.09.007.

Allstadt, K. E., Matoza, R. S., Lockhart, A. B., Moran, S. C., Caplan-Auerbach, J., Haney, M. M., Thelen, W. A., and Malone, S. D. Seismic and acoustic signatures of surficial mass movements at volcanoes. *Journal of Volcanology and Geothermal Research*, 364:76–106, 2018b. doi: 10.1016/j.jvolgeores.2018.09.007.

Bahavar, M., Allstadt, K. E., Van Fossen, M., Malone, S. D., and Trabant, C. Exotic seismic events catalog (esec) data product. *Seismological Research Letters*, 90(3):1355–1363, 2019. doi: 10.1785/0220180402.

Bartlow, N. M. A long-term view of episodic tremor and slip in cascadia. *Geophysical Research Letters*, 47(3):e2019GL085303, 2020. doi: 10.1029/2019GL085303.

Bergen, K. J., Johnson, P. A., de Hoop, M. V., and Beroza, G. C. Machine learning for data-driven discovery in solid earth geoscience. *Science*, 363(6433):eaau0323, 2019. doi: 10.1126/science.aau0323.

Braun, T., Frigo, B., Chiaia, B., Bartelt, P., Famiani, D., and Wassermann, J. Seismic signature of the deadly snow avalanche of january 18, 2017, at rigopiano (italy). *Scientific reports*, 10(1):1–10, 2020. doi: 10.1038/s41598-020-75368-z.

Cascades Volcano Observatory/USGS. Cascade chain volcano monitoring, 2001.

Chmiel, M., Walter, F., Wenner, M., Zhang, Z., McArdell, B. W., and Hibert, C. Machine learning improves debris flow warning. *Geophysical Research Letters*, 48(3):e2020GL090874, 2021. doi: 10.1029/2020GL090874.

Collette, A., Kluyver, T., Caswell, T. A., Tocknell, J., Kieffer, J., Scopatz, A., Dale, D., Chen, Jelenak, A., payno, juliagarriga, VINCENT, T., Sciarelli, P., Valls, V., Ghosh, S., Pedersen, U. K., jakirkham, Raspaud, M., Parsons, A., Abbasi, H., Readey, J., Paramonov, A., Chan, L., Solé, V. A., jialin, Danilevski, C., Feng, Y., Vaillant, G. A., Teichmann, M., and Brucher, M. h5py/h5py: 3.2.1, Mar. 2021.

Collins, E., Allstadt, K., Groult, C., Hibert, C., Malet, J., Toney, L., and Bessette-Kirton, E. Seismogenic landslides and other mass movements: Us geological survey data release, 2022.

Crosson, R. S. Small earthquakes, structure, and tectonics of the puget sound region. *Bulletin of the Seismological Society of America*, 62 (5):1133–1171, 1972. doi: 10.1785/BSSA0620051133.

Deng, J., Dong, W., Socher, R., Li, L.-J., Li, K., and Fei-Fei, L. Imagenet: A large-scale hierarchical image database. In *2009 IEEE conference on computer vision and pattern recognition*, pages 248–255. Ieee, 2009. doi: 10.1109/CVPR.2009.5206848.

Dragert, H., Wang, K., and James, T. S. A silent slip event on the deeper cascadia subduction interface. *Science*, 292(5521):1525–1528, 2001. doi: 10.1126/science.1060152.

Ducellier, A. and Creager, K. C. An 8-year-long low-frequency earthquake catalog for southern cascadia. *Journal of Geophysical Research: Solid Earth*, 127(4):e2021JB022986, 2022. doi: 10.1029/2021JB022986.

Feng, Z.-y. The seismic signatures of the surge wave from the 2009 xiaolin landslide-dam breach in taiwan. *Hydrological Processes*, 26(9): 1342–1351, 2012. doi: 10.1002/hyp.8239.

Gene A. Ichinose, Hong Kie Thio, P. G. S. Rupture process and near-source shaking of the 1965 seattle-tacoma and 2001 nisqually, intraslab earthquakes. *Geophysical Research Letters*, 31(10):1–4, 2004. doi: 10.1029/2004GL019668.

Gomberg, J. and Bodin, P. The productivity of cascadia aftershock sequences. *Bulletin of the Seismological Society of America*, 111(3): 1494–1507, 2021. doi: 10.1785/0120200344.

Gomberg, J., Sherrod, B., Trautman, M., Burns, E., and Snyder, D. Contemporary seismicity in and around the yakima fold-and-thrust belt in eastern washington. *Bulletin of the Seismological Society of America*, 102(1):309–320, 2012. doi: 10.1785/0120110065.

Harris, C. R., Millman, K. J., Van Der Walt, S. J., Gommers, R., Virtanen, P., Cournapeau, D., Wieser, E., Taylor, J., Berg, S., Smith, N. J., et al. Array programming with numpy. *Nature*, 585(7825):357–362, 2020. doi: 10.1038/s41586-020-2649-2.

Hartog, J., Friberg, P., Kress, V., Bodin, P., and Bhadha, R. Open-source anss quake monitoring system software. *Seismological Research Letters*, 91:677–686, 2019. doi: 10.1785/0220190219.

Hayes, G. Slab2 - A Comprehensive Subduction Zone Geometry Model, 2018. Type: dataset.

Hearne, M. and Schovanec, H. E. libcomcat Software Release, 2020. Medium: Other.

Herrmann, R. B. Fasthypo-a hypocenter location program. *Earthquake notes*, 50(2):25–38, 1979. doi: 10.1785/gssrl.50.2.25.

Hibert, C., Ekström, G., and Stark, C. P. Dynamics of the bingham canyon mine landslides from seismic signal analysis. *Geophysical research letters*, 41(13):4535–4541, 2014. doi: 10.1002/2014GL060592.

Hibert, C., Michéa, D., Provost, F., Malet, J.-P., and Geertsema, M. Exploration of continuous seismic recordings with a machine learning approach to document 20 yr of landslide activity in alaska. *Geophysical Journal International*, 219(2):1138–1147, 07 2019. doi: 10.1093/gji/ggz354.

Hunter, J. D. Matplotlib: A 2d graphics environment. *Computing in science & engineering*, 9(03):90–95, 2007. doi: 10.1109/MCSE.2007.55.

Hutko, A. R., Bahavar, M., Trabant, C., Weekly, R. T., Fossen, M. V., and Ahern, T. Data products at the iris-dmc: Growth and usage. *Seismological Research Letters*, 88(3):892–903, 2017. doi: 10.1785/0220160190.

IRIS Transportable Array. Usarray transportable array, 2003.

Jennings, P. C. and Kanamori, H. Effect of distance on local magnitudes found from strong-motion records. *Bulletin of the Seismological Society of America*, 73(1):265–280, 1983. doi: 10.1785/BSSA0730010265.

Kingma, D. P. and Ba, J. Adam: A Method for Stochastic Optimization. 2014. doi: 10.48550/ARXIV.1412.6980. Publisher: arXiv Version Number: 9.

Klein, F. W. User's guide to hypoinverse-2000, a fortran program to solve for earthquake locations and magnitudes. Technical report, US Geological Survey, 2002.

Kong, Q., Trugman, D. T., Ross, Z. E., Bianco, M. J., Meade, B. J., and Gerstoft, P. Machine learning in seismology: Turning data into insights. *Seismological Research Letters*, 90(1):3–14, 2019. doi: 10.1785/0220180259.

Koper, K. D., Holt, M. M., Voyles, J. R., Burlacu, R., Pyle, M. L., Wang, R., and Schmandt, B. Discrimination of Small Earthquakes and Buried Single-Fired Chemical Explosions at Local Distances (<150 km) in the Western United States from Comparison of Local Magnitude (ML) and Coda Duration Magnitude (MC). *Bulletin of the Seismological Society of America*, 111(1):558–570, 10 2020. doi: 10.1785/0120200188.

Krischer, L., Megies, T., Barsch, R., Beyreuther, M., Lecocq, T., Caudron, C., and Wassermann, J. ObsPy: a bridge for seismology into the scientific Python ecosystem. *Computational Science & Discovery*, 8(1):014003, May 2015. doi: 10.1088/1749-4699/8/1/014003.

Luna, L. V. and Korup, O. Seasonal landslide activity lags annual precipitation pattern in the pacific northwest. *Geophysical Research Letters*, 49(18):e2022GL098506, 2022. doi: 10.1029/2022GL098506. e2022GL098506 2022GL098506.

Malfante, M., Dalla Mura, M., Métaxian, J.-P., Mars, J. I., Macedo, O., and Inza, A. Machine learning for volcano-seismic signals: Challenges and perspectives. *IEEE Signal Processing Magazine*, 35(2):20–30, 2018. doi: 10.1109/MSP.2017.2779166.

Manconi, A., Gariano, S. L., Coviello, V., and Guzzetti, F. How many rainfall-induced landslides are detectable by a regional seismic monitoring network? In *Workshop on World Landslide Forum*, pages 161–168. Springer, 2017. doi: 10.1007/978-3-319-53487-9_18.

Michelini, A., Cianetti, S., Gaviano, S., Giunchi, C., Jozinovic, D., and Lauciani, V. INSTANCE - the Italian seismic dataset for machine learning. *Earth System Science Data*, May 2021. doi: 10.5194/essd-2021-164.

Mousavi, S. M. and Beroza, G. C. Deep-learning seismology. *Science*, 377(6607):eabm4470, 2022. doi: 10.1126/science.abm4470.

Mousavi, S. M., Sheng, Y., Zhu, W., and Beroza, G. C. Stanford earthquake dataset (stead): A global data set of seismic signals for ai. *IEEE Access*, 7:179464–179476, 2019. doi: 10.1109/ACCESS.2019.2947848.

Mousavi, S. M., Ellsworth, W. L., Zhu, W., Chuang, L. Y., and Beroza, G. C. Earthquake transformer—an attentive deep-learning model for simultaneous earthquake detection and phase picking. *Nature communications*, 11(1):1–12, 2020. doi: 10.1038/s41467-020-17591-w.

Münchmeyer, J., Woollam, J., Rietbrock, A., Tilmann, F., Lange, D., Bornstein, T., Diehl, T., Giunchi, C., Haslinger, F., Jozinović, D., et al. Which picker fits my data? a quantitative evaluation of deep learning based seismic pickers. *Journal of Geophysical Research: Solid Earth*, 127 (1):e2021JB023499, 2022. doi: 10.1029/2021JB023499.

Natural Resources Canada (NRCAN Canada). Canadian national seismograph network, 1975.

Ni, Y. niyiyu/pnw-ml: Pnw-ml seismic dataset, Feb. 2023.

Paullada, A., Raji, I. D., Bender, E. M., Denton, E., and Hanna, A. Data and its (dis)contents: A survey of dataset development and use in machine learning research. *Patterns*, 2(11):100336, 2021. doi: https://doi.org/10.1016/j.patter.2021.100336.

Richter, C. F. Elementary seismology. 1958.

Rogers, G. and Dragert, H. Episodic tremor and slip on the cascadia subduction zone: The chatter of silent slip. *science*, 300(5627):1942–1943, 2003. doi: 10.1126/science.1084783.

Rutgers University. Ocean observatories initiative, 2013.

SCEDC. Southern California Earthquake Data Center, 2013. Type: dataset.

Schorlemmer, D., Euchner, F., Kästli, P., Saul, J., Group, Q. W., et al. Quakeml: status of the xml-based seismological data exchange format. *Annals of Geophysics*, 54(1), 2011. doi: 10.4401/ag-4874.

Survey, U. S. G. Advanced National Seismic System (ANSS) Comprehensive Catalog. 2017. doi: 10.5066/F7MS3QZH. Publisher: U.S. Geological Survey.

Uieda, L., Tian, D., Leong, W. J., Toney, L., Schlitzer, W., Grund, M., Newton, T., Ziebarth, M., Jones, M., and Wessel, P. PyGMT: A Python interface for the Generic Mapping Tools, Feb. 2021. The development of PyGMT has been supported by NSF grants OCE-1558403 and EAR-1948603.

University of Oregon. Pacific northwest seismic network - university of oregon, 1990.

University of Washington. Pacific northwest seismic network - university of washington, 1963.

Wang, A., Singh, A., Michael, J., Hill, F., Levy, O., and Bowman, S. R. Glue: A multi-task benchmark and analysis platform for natural language understanding. *arXiv preprint arXiv:1804.07461*, 2018.

Wang, R., Schmandt, B., Holt, M., and Koper, K. Advancing local distance discrimination of explosions and earthquakes with joint p/s and ml-mc classification. *Geophysical Research Letters*, 48(23):e2021GL095721, 2021. doi: 10.1029/2021GL095721.

Wech, A. G. and Bartlow, N. M. Slip rate and tremor genesis in cascadia. *Geophysical Research Letters*, 41(2):392–398, 2014.

doi: 10.1002/2013GL058607.

Wech, A. G., Creager, K. C., Houston, H., and Vidale, J. E. An earthquake-like magnitude-frequency distribution of slow slip in northern cascadia. *Geophysical Research Letters*, 37(22), 2010. doi: 10.1029/2010GL044881.

Wiemer, S. and Wyss, M. Minimum magnitude of completeness in earthquake catalogs: Examples from alaska, the western united states, and japan. *Bulletin of the Seismological Society of America*, 90(4):859–869, 2000. doi: 10.1785/0119990114.

Witter, R. C., Kelsey, H. M., and Hemphill-Haley, E. Great cascadia earthquakes and tsunamis of the past 6700 years, coquille river estuary, southern coastal oregon. *Geological Society of America Bulletin*, 115(10):1289–1306, 2003. doi: 10.1130/B25189.1.

Woollam, J., Rietbrock, A., Bueno, A., and De Angelis, S. Convolutional Neural Network for Seismic Phase Classification, Performance Demonstration over a Local Seismic Network. *Seismological Research Letters*, 90(2A):491–502, Mar. 2019. doi: 10.1785/0220180312.

Woollam, J., Münchmeyer, J., Tilmann, F., Rietbrock, A., Lange, D., Bornstein, T., Diehl, T., Giunchi, C., Haslinger, F., Jozinović, D., et al. Seisbench—a toolbox for machine learning in seismology. *Seismological Society of America*, 93(3):1695–1709, 2022. doi: 10.1785/0220210324.

Yan, Y., Cui, Y., Tian, X., Hu, S., Guo, J., Wang, Z., Yin, S., and Liao, L. Seismic signal recognition and interpretation of the 2019 "7.23" shuicheng landslide by seismogram stations. *Landslides*, 17(5):1191–1206, 2020. doi: 10.1007/s10346-020-01358-x.

Zhu, W., Mousavi, S. M., and Beroza, G. C. Seismic signal augmentation to improve generalization of deep neural networks. In *Advances in geophysics*, volume 61, pages 151–177. Elsevier, 2020. doi: 10.1016/bs.agph.2020.07.003.

Supplementary Materials: Curated Pacific Northwest AI-ready Seismic Dataset

Yiyu Ni *[1], **Alexander R. Hutko**[1,2], **Francesca Skene**[1], **Marine A. Denolle**[1], **Stephen D. Malone**[1,2], **Paul Bodin**[1,2], **J. Renate Hartog**[1,2], **Amy K. Wright**[1,2]

[1]Department of Earth and Space Sciences, University of Washington, Seattle, WA, [2]Pacific Northwest Seismic Network, Seattle, WA

AQMS event type use by the PNSN	ComCat label	Description
eq		earthquake
le		local earthquake
re		regional earthquake
ts	**earthquake**	teleseism
se		slow earthquake
lp		long period volcanic earthquake
lf		low-frequency event
ex		generic chemical blast
px	**explosion**	unconfirmed blast or explosion
sh		refraction/reflection survey shot
su	**surface event**	surface event
th	**thunder**	thunder
sn	**sonic boom**	sonic shockwave
pc	**plane crash**	plane crash
qb	quarry blast	quarry blast
nt	nuclear explosion	nuclear test
ve	volcanic eruption	volcanic eruption
co	mine collapse	mine/tunnel collapse
df	debris avalanche	debris flow/avalanche
av	snow avalanche	snow/ice avalanche
ls	landslide	landslide
rb	rock burst	rockburst
rs	rockslide	rockslide
bc	building collapse	building collapse/demolition
mi	meteor impact	meteor/comet impact
uk	unknown	unknown type

Table S1 The event types and labels used in PNSN's ANSS Quake Monitoring System (AQMS). Several event types are merged into one when being reported to the ComCat.

*Corresponding author: niyiyu@uw.edu

UTC Time	CISN Event ID	PNSN Event ID	Magnitude
2022-12-20 10:34:24	nc73821036	uw61899256	Mw 6.4
2022-12-20 10:52:39	nc73821106	uw61899266	Ml 3.1
2022-12-20 11:42:54	nc73821226	uw61899301	Ml 3.0
2022-12-20 12:21:43	nc73821346	uw61899311	Ml 3.0
2022-12-20 13:35:06	nc73821486	uw61899326	Ml 3.4
2022-12-20 13:53:19	nc73821516	uw61899331	Ml 3.3
2022-12-20 15:09:05	nc73821636	uw61899336	Mw 4.0
2022-12-20 15:30:01	nc73821656	uw61899346	Ml 3.0
2022-12-20 16:33:41	nc73821761	uw61899381	Ml 3.2
2022-12-20 22:06:34	nc73822026	uw61890602	Mw 4.4
2022-12-21 01:07:33	nc73822146	uw61890647	Ml 3.0
2022-12-21 07:17:15	nc73822341	uw61890697	Ml 3.0
2022-12-21 16:28:16	nc73822556	uw61890767	Ml 3.3
2022-12-22 08:47:13	nc73822961	uw61890997	Ml 3.3
2022-12-22 11:49:55	nc73823036	uw61891007	Mw 3.8
2022-12-24 19:33:44	nc73824236	uw61900186	Mw 4.2
2022-12-25 19:40:29	nc73824826	uw61900336	Md 3.0
2022-12-29 00:16:18	nc73826156	uw61900806	Md 3.0
2023-01-01 18:35:04	nc73827571	uw61901146	Mw 5.4
2023-01-06 12:27:19	nc73829331	uw61901521	Ml 3.3

Table S2 The events selected from the 20 December 2022 Northern California earthquake sequence that are included in the data set. Source origin time, event ID, and magnitude are reported by the California Integrated Seismic Network (CISN), with corresponding PNSN event ID.

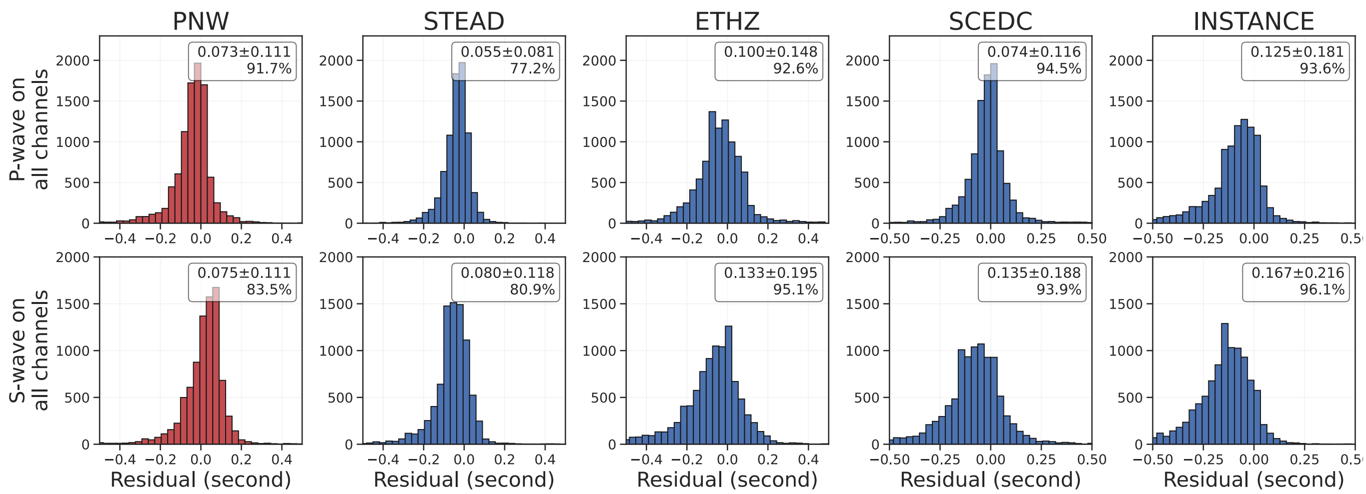

Figure S1 Histogram of P- and S-wave picking residuals ($t_{ML} - t_{PNSN}$) from the benchmark testing on strong motion channels. The number in the upper right corner of each subplot shows the mean absolute error (MAE), the root-mean-square error (RMSE), the mean value of the residual, and the picking completeness in percentage with respect to the ground truth. The PNW-retrained Earthquake Transformer outperforms than other four pre-trained models from SeisBench (Woollam et al., 2022) in both picking accuracy and detecting completeness.

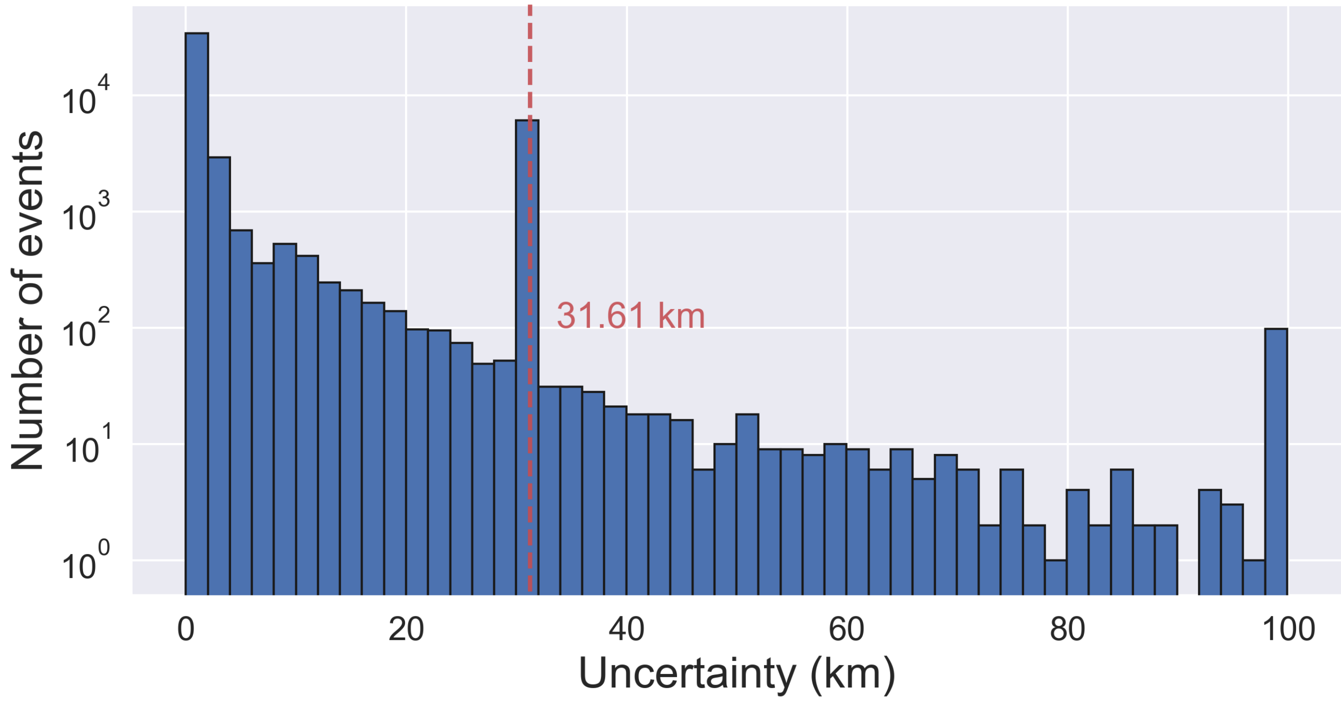

Figure S2 Histogram of depth uncertainties of ComCat events in log scale. A large number of events with 31.61 km depth uncertainty mostly come from locating a probable explosion event with a fixed depth.

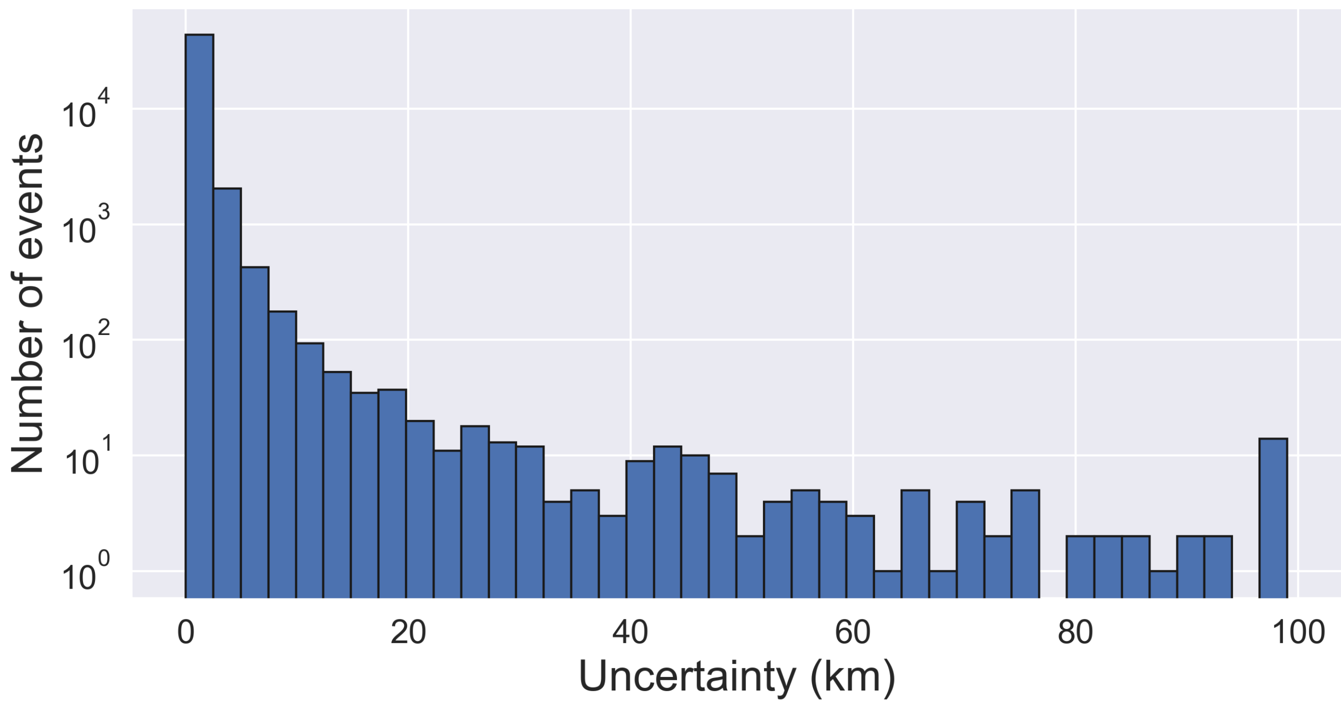

Figure S3 Histogram of horizontal uncertainties of ComCat events in log scale.

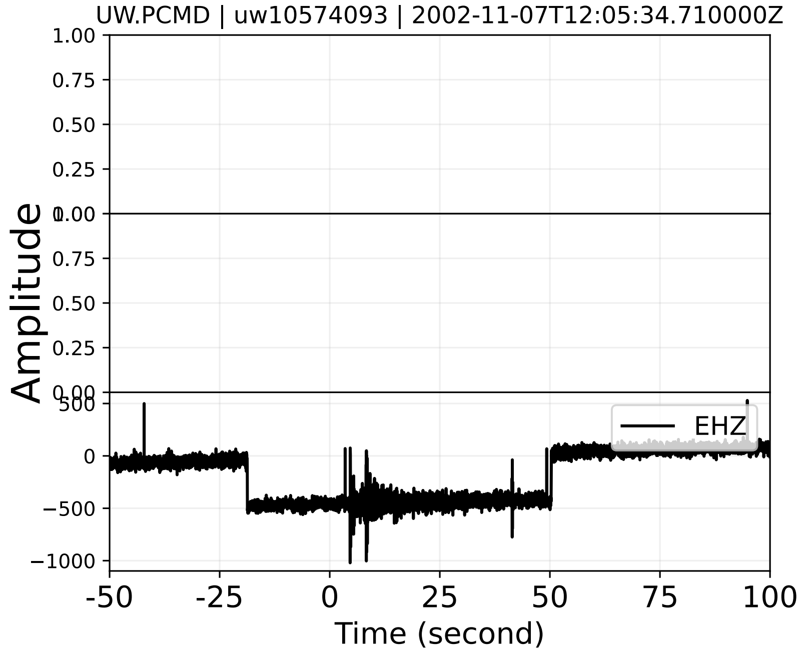

Figure S4 Example of a stream with a step offset from short-period EH channel. FDSN network and station code, ComCat event ID, and source origin time are labeled on the top.

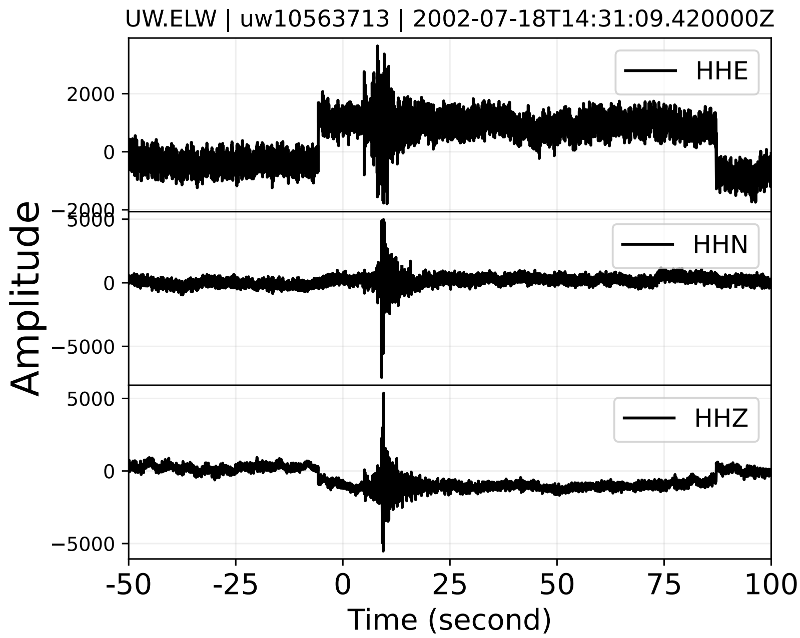

Figure S5 Example of a stream with a step offset from board-band HH channel. FDSN network and station code, ComCat event ID, and source origin time are labeled on the top.

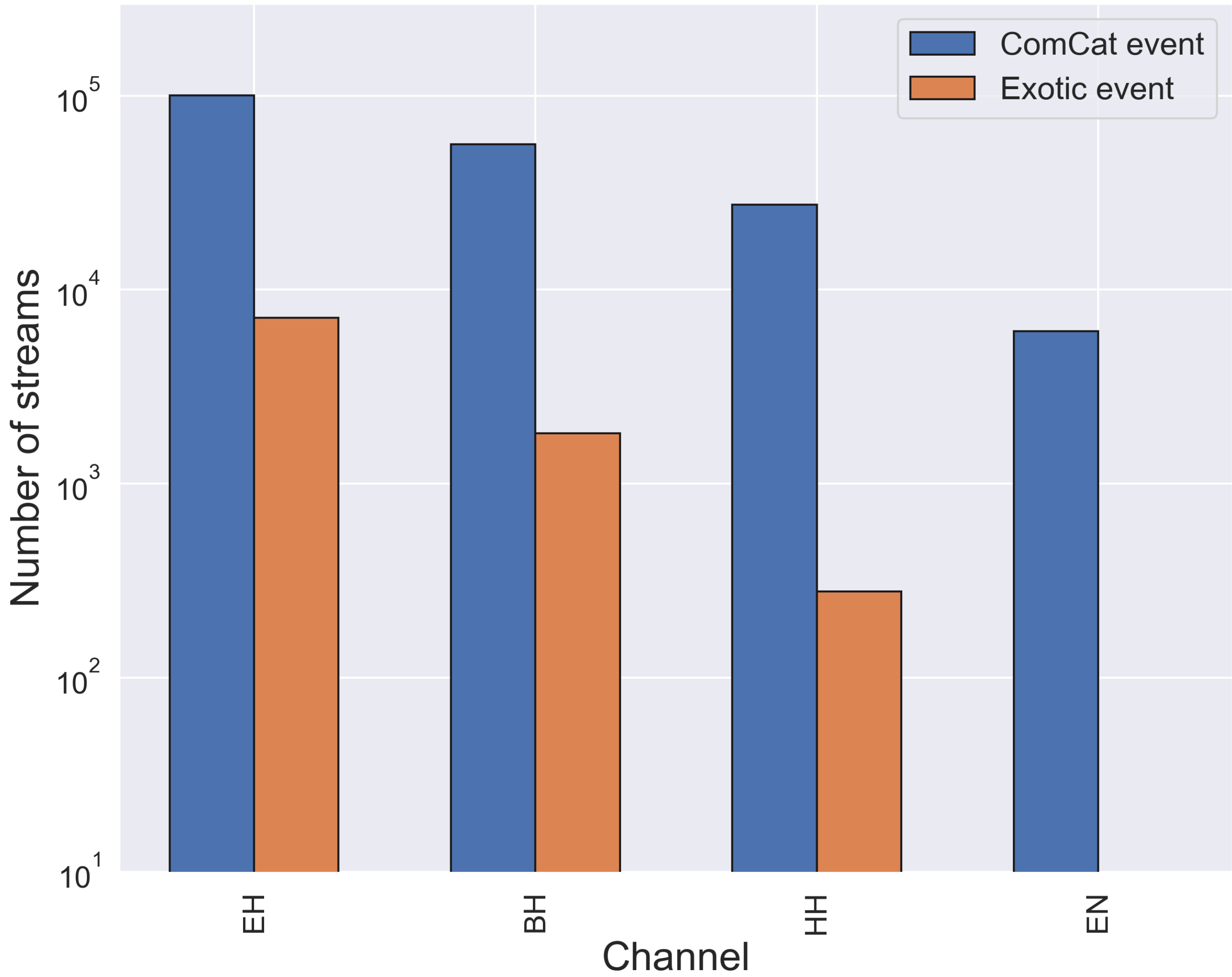

Figure S6 Number of streams arranged by the instrument type.

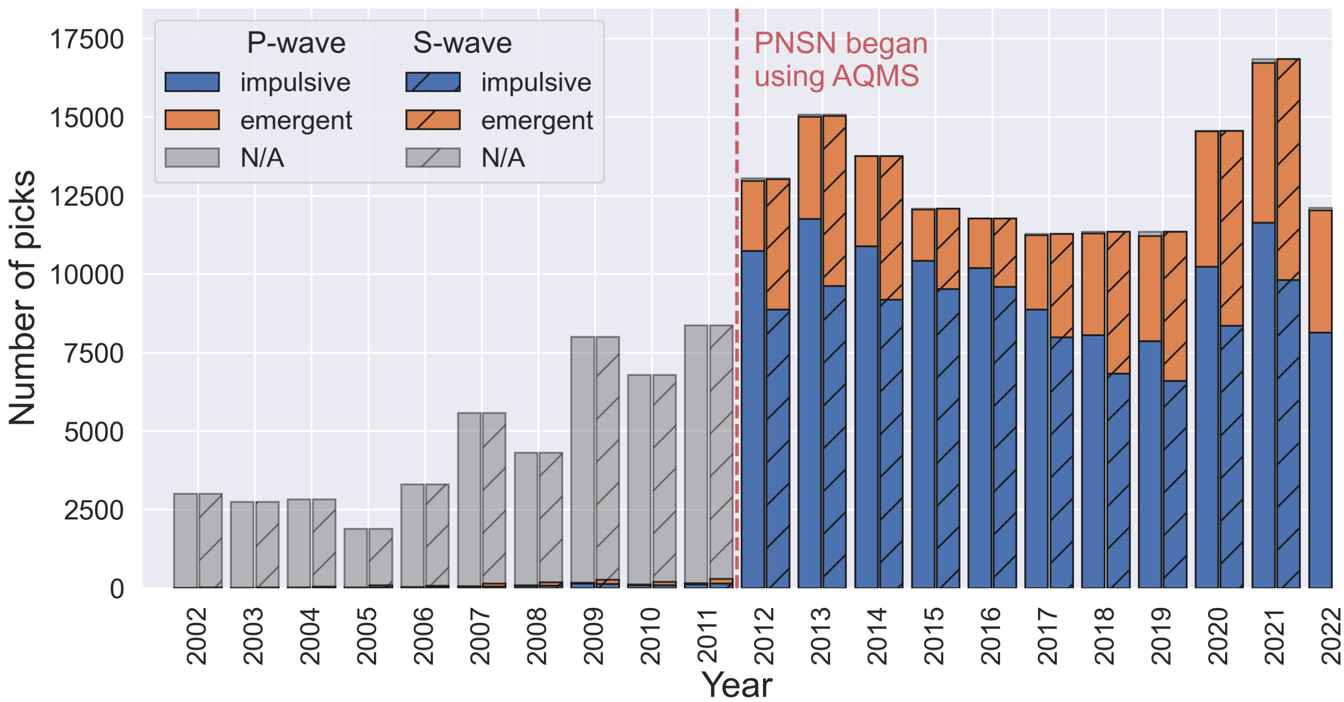

Figure S7 Number of picked P- and S-waves onsets as a function of time from ComCat events.

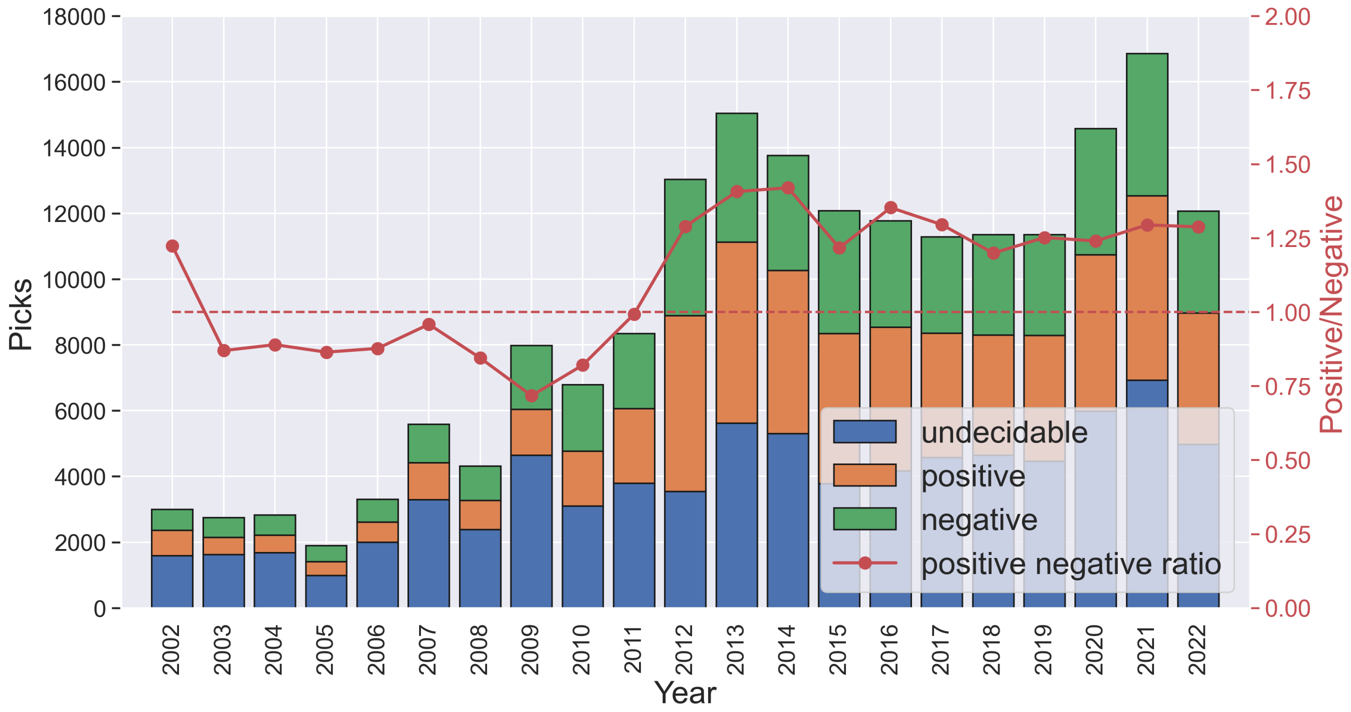

Figure S8 Number of picked P-wave polarity as a function of time. The red line marks the positive-negative ratio of the P-wave polarities.

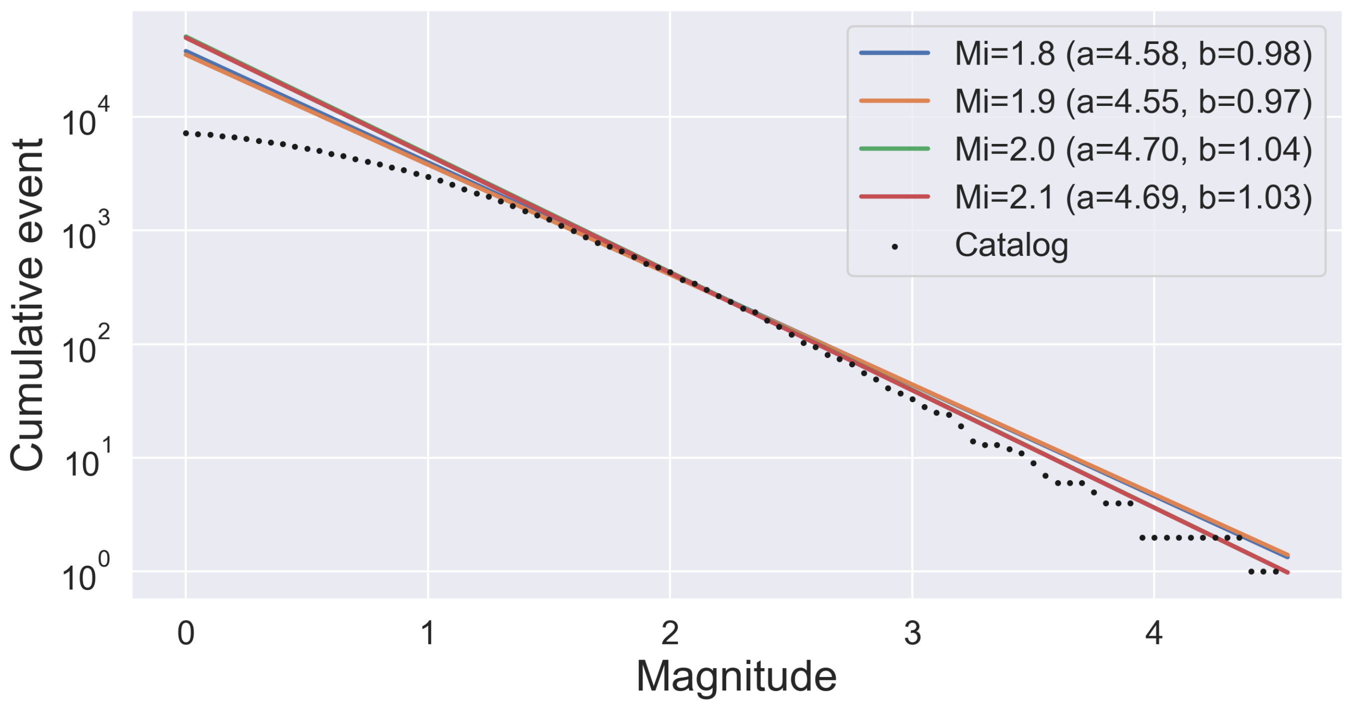

Figure S9 Fitting of Gutenberg-Richter (GR) power law distribution of magnitudes (solid lines) with 3 years of earthquake events cataloged by PNSN (black dots). The plot indicates that the minimum magnitude of completeness is around 2.

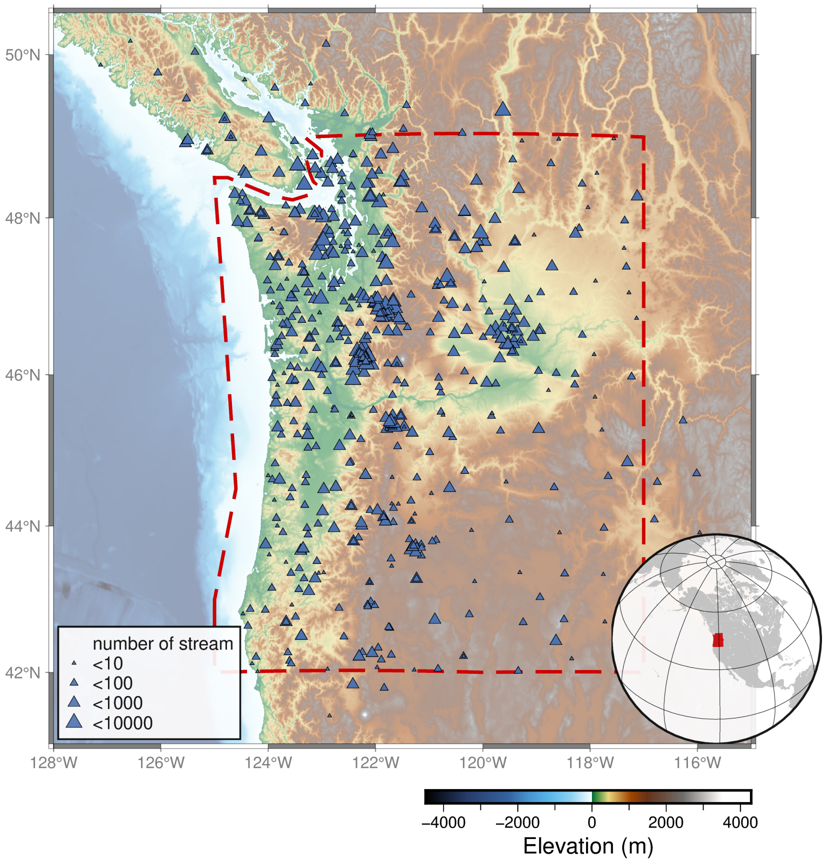

Figure S10 Number of streams from the ComCat event catalog per station. The red dashed polygon denotes the authoritative region boundaries of PNSN.

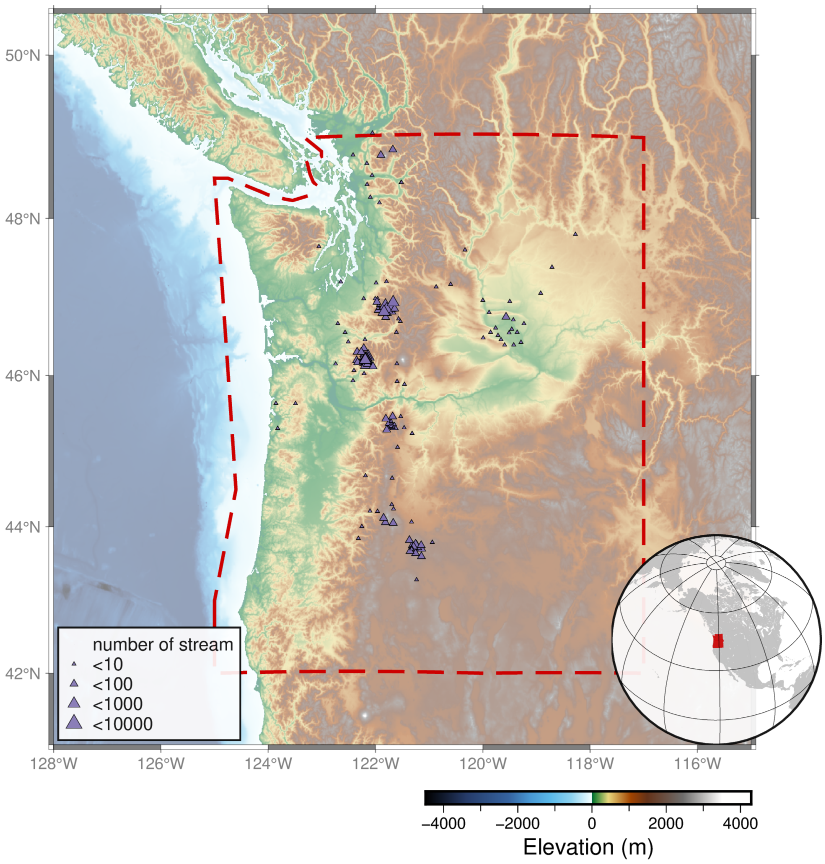

Figure S11 Number of streams from the Exotic event catalog per station. The red dashed polygon denotes the authoritative region boundaries of PNSN. Note that 96% of the exotic events are surface events.

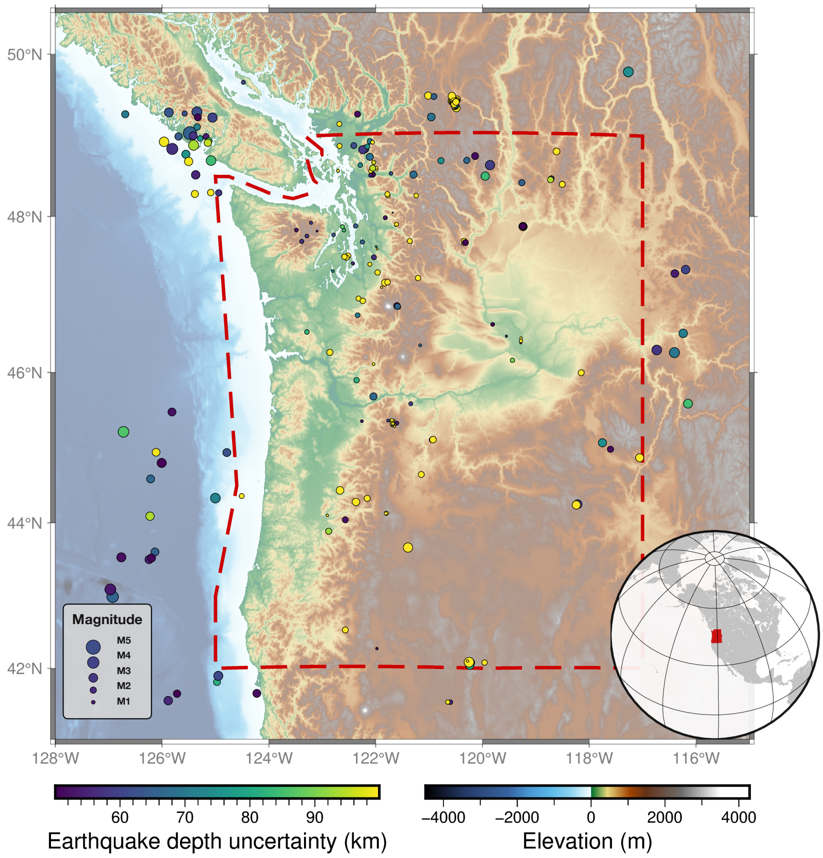

Figure S12 Location of the events with location horizontal uncertainty larger than 20 km. The red polygon denotes the authoritative region boundaries of PNSN.

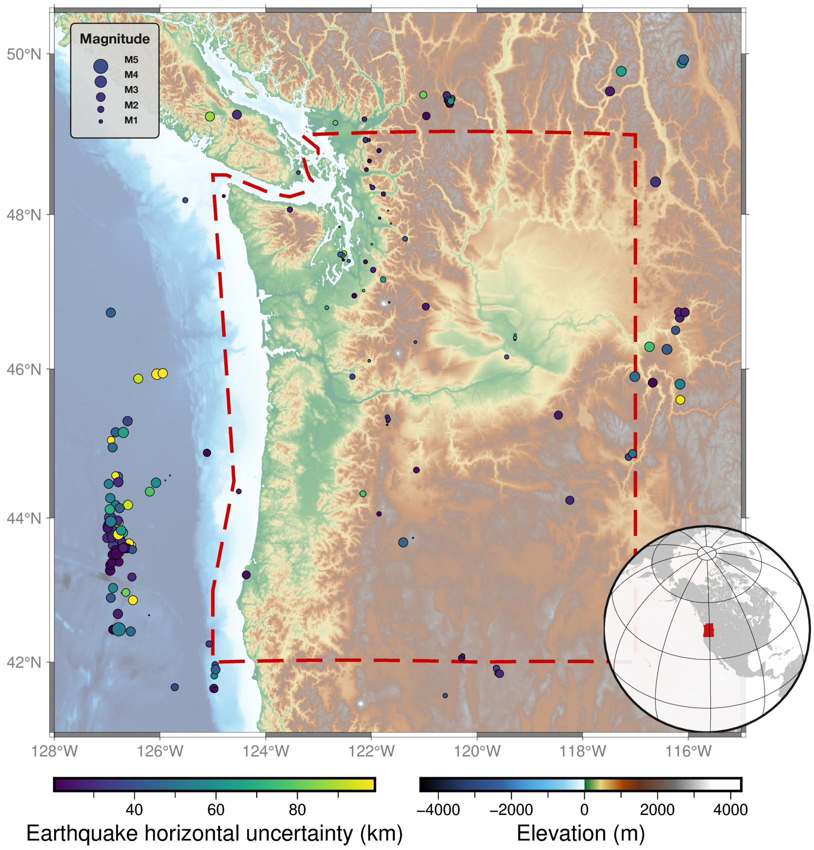

Figure S13 Location of the events with location horizontal uncertainty larger than 20 km. The red polygon denotes the authoritative region boundaries of PNSN.

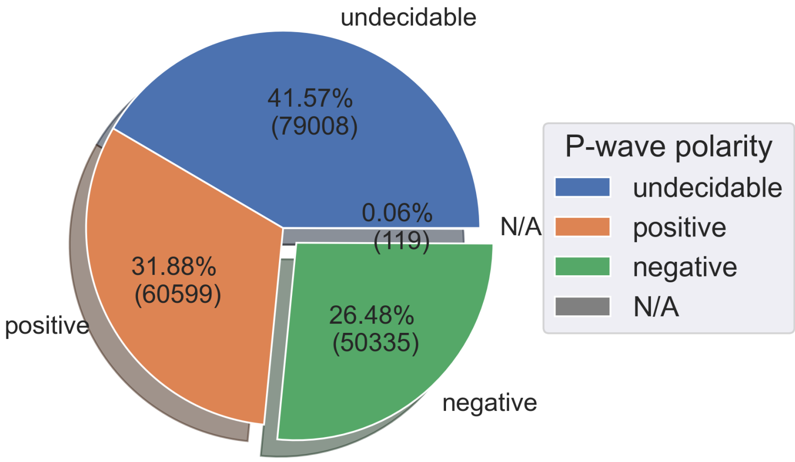

Figure S14 Percentages of the picked P-wave polarity of all streams from ComCat events.

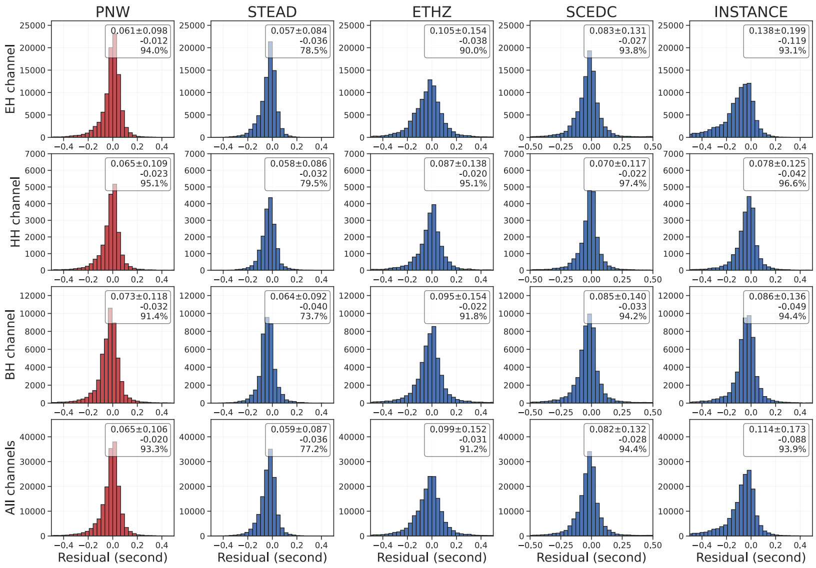

Figure S15 Histogram of P-wave picking residuals on velocity channels. The number in the upper right corner of each figure shows the mean absolute error, the root mean square error of the residual, and the picking completeness in percentage with respect to the ground truth.

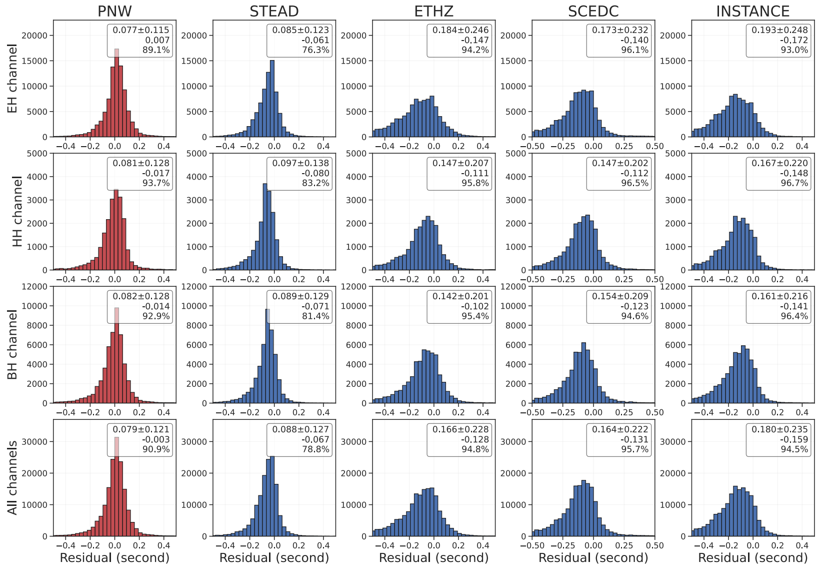

Figure S16 Histogram of S-wave picking residuals on velocity channels. The number in the upper right corner of each figure shows the mean absolute error, the root mean square error of the residual, and the picking completeness in percentage with respect to the ground truth.

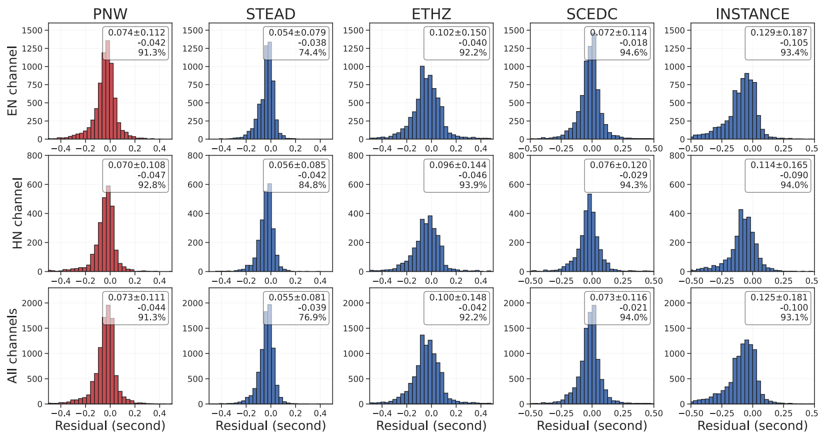

Figure S17 Histogram of P-wave picking residuals on strong motion channels. The number in the upper right corner of each figure shows the mean absolute error, the root mean square error of the residual, and the picking completeness in percentage with respect to the ground truth.

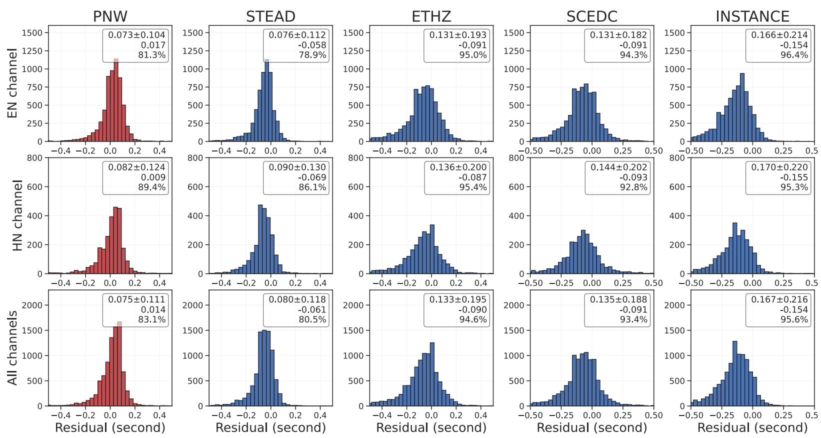

Figure S18 Histogram of S-wave picking residuals on strong-motion channels. The number in the upper right corner of each figure shows the mean absolute error, the root mean square error of the residual, and the picking completeness in percentage with respect to the ground truth.

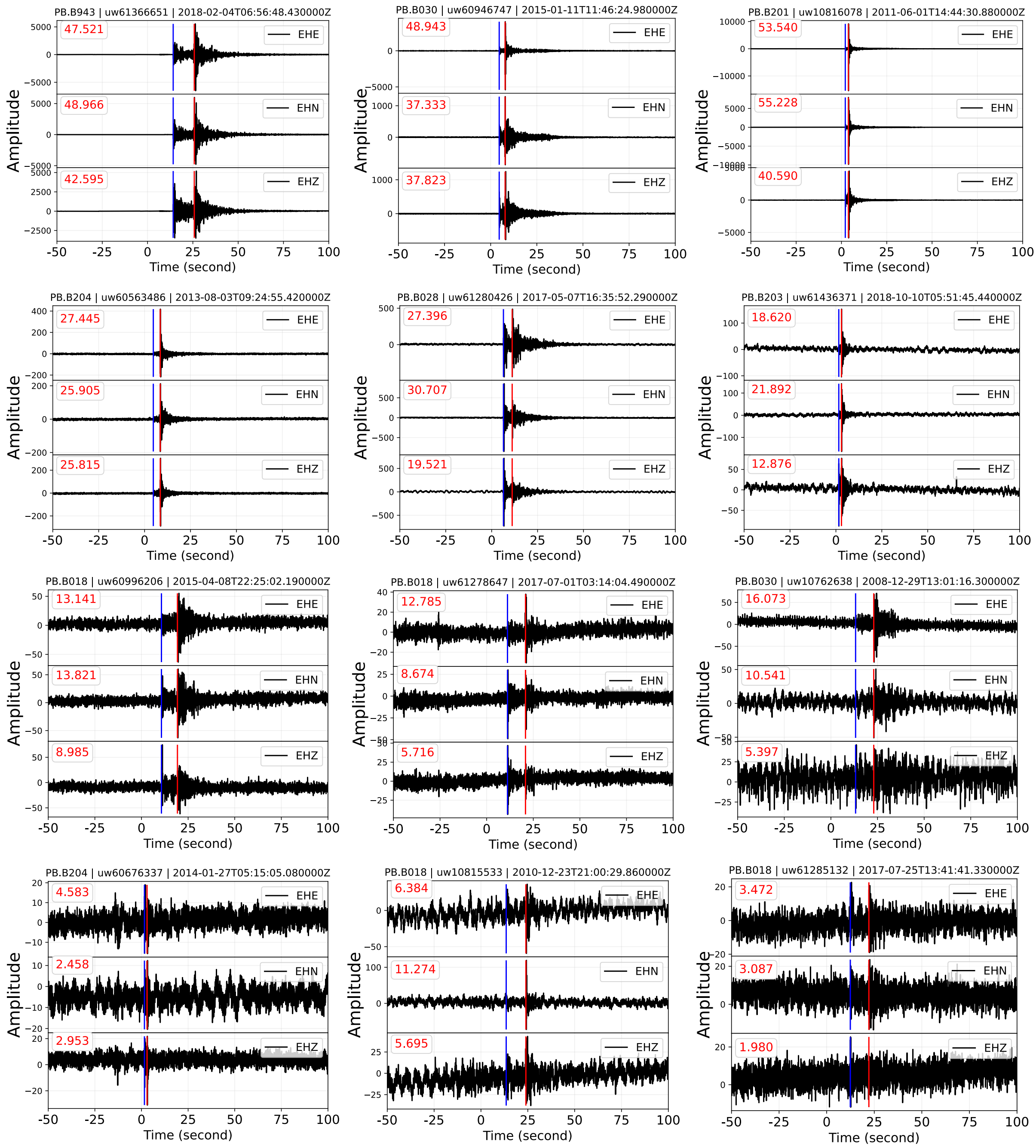

Figure S19 Randomly selected waveform samples of ComCat earthquake events from short-period three-component EH? channels. SNRs are marked on the upper left for each component. The blue line marks the P-wave arrival, and the red line (if any) marks the S-wave arrival.

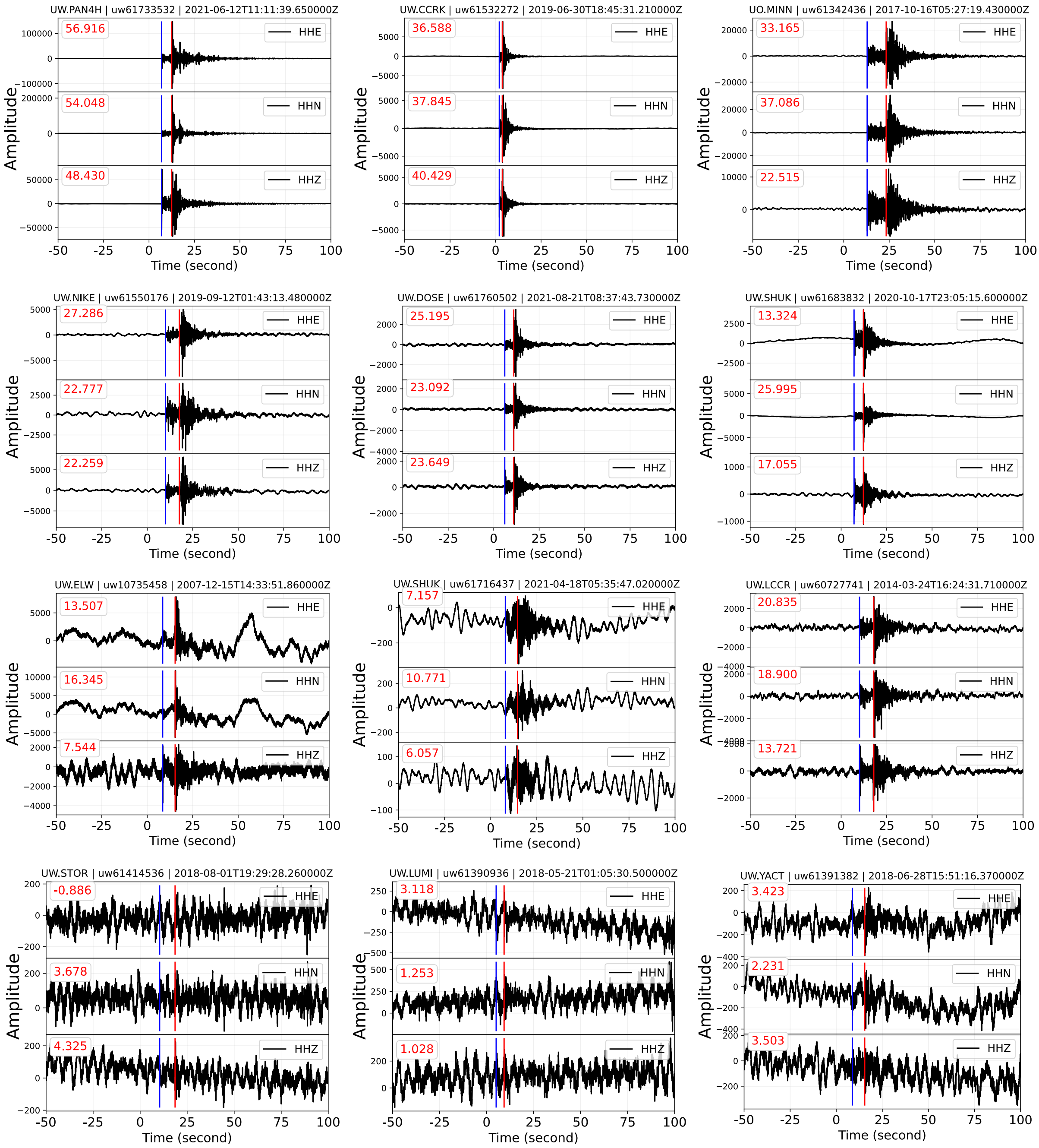

Figure S20 Randomly selected waveform samples of ComCat earthquake events from board-band three-component HH? channels. SNRs are marked on the upper left for each component. The blue line marks the P-wave arrival, and the red line (if any) marks the S-wave arrival.

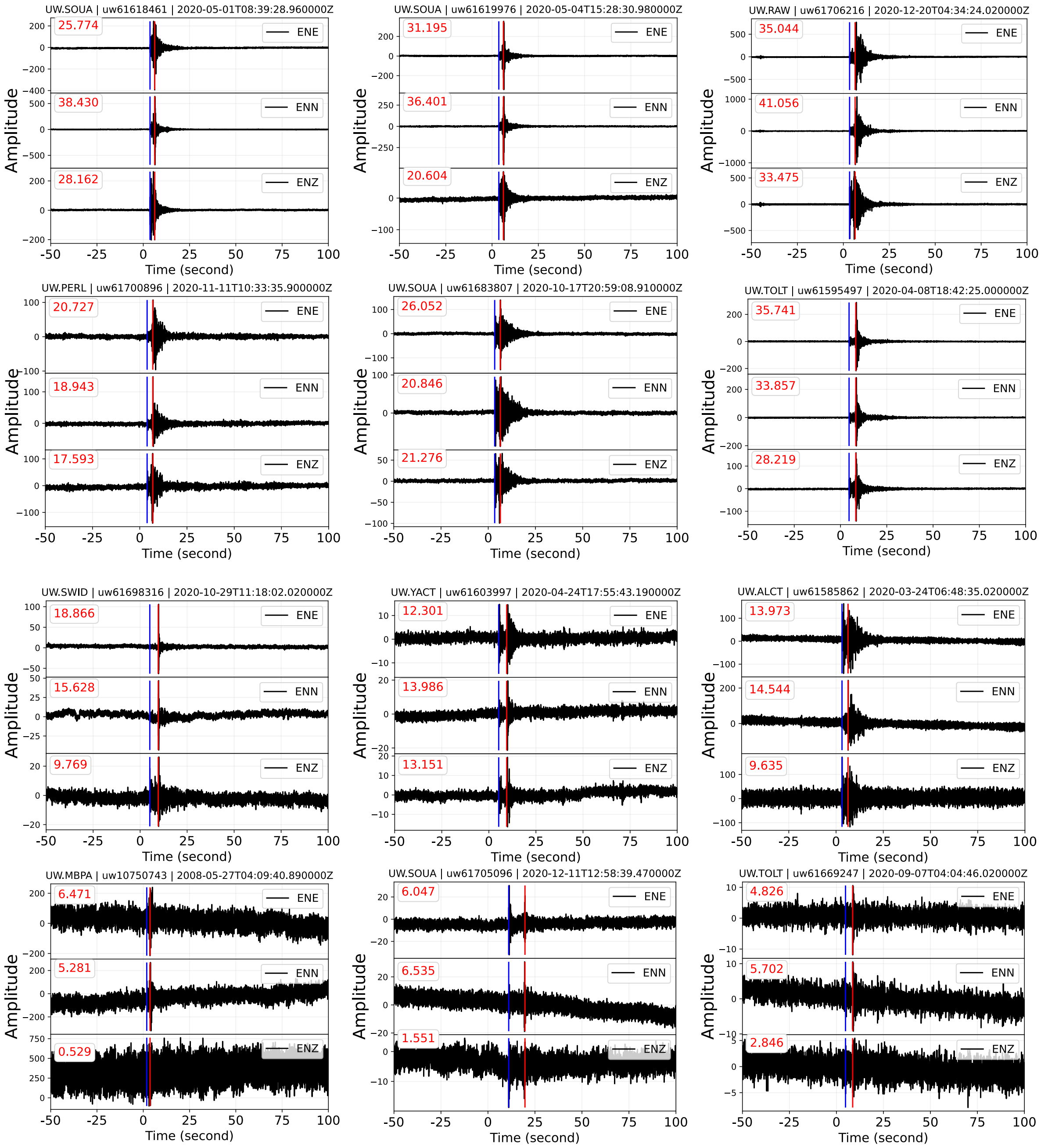

Figure S21 Randomly selected waveform samples of ComCat earthquake events from strong-motion EN? channels. SNRs are marked on the upper left for each component. The blue line marks the P-wave arrival, and the red line (if any) marks the S-wave arrival.

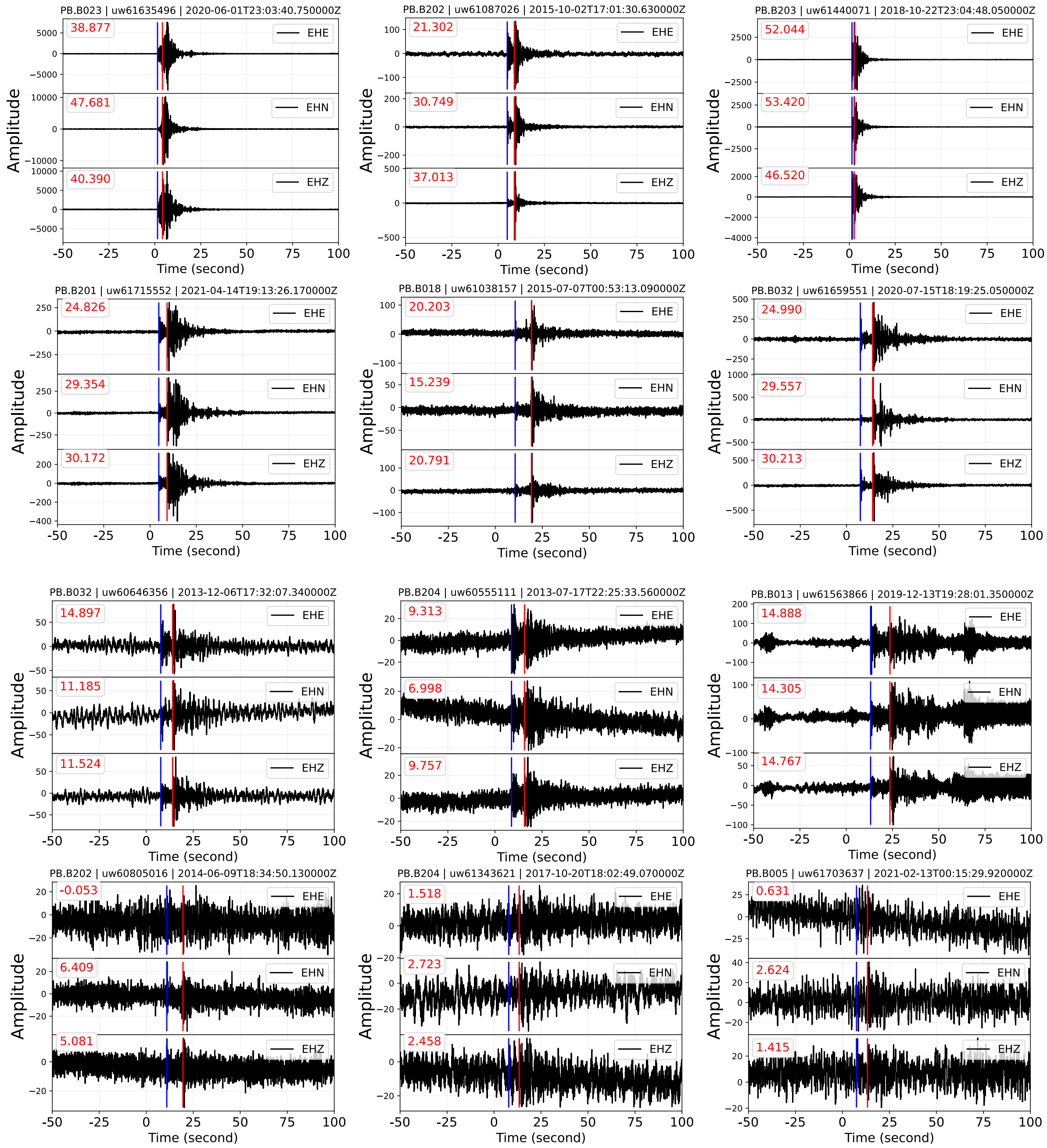

Figure S22 Randomly selected waveform samples of ComCat explosion events from short-period three-component EH? channels. SNRs are marked on the upper left for each component. The blue line marks the P-wave arrival, and the red line (if any) marks the S-wave arrival.

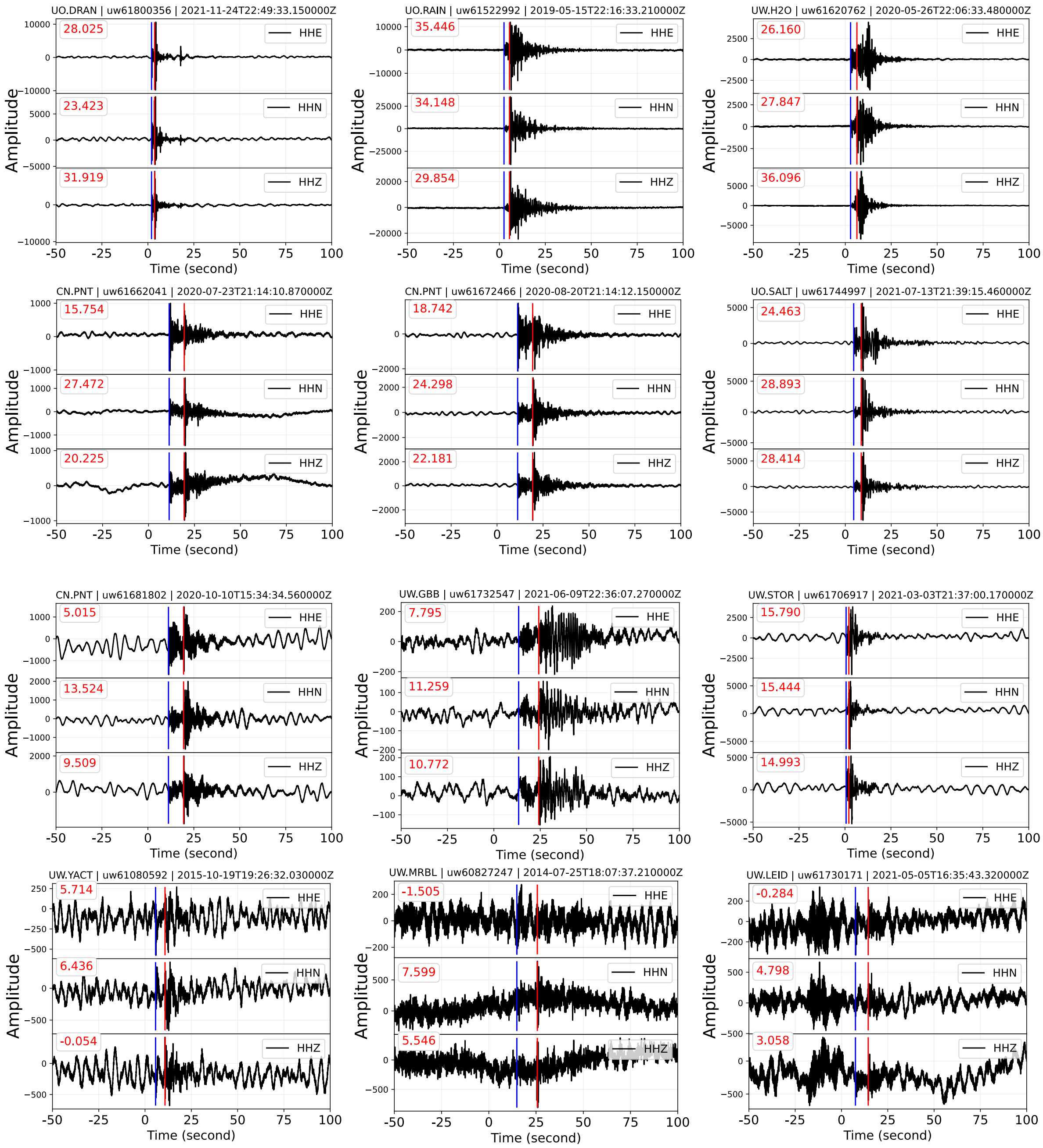

Figure S23 Randomly selected waveform samples of ComCat explosion events from board-band three-component HH? channels. SNRs are marked on the upper left for each component. The blue line marks the P-wave arrival, and the red line (if any) marks the S-wave arrival.

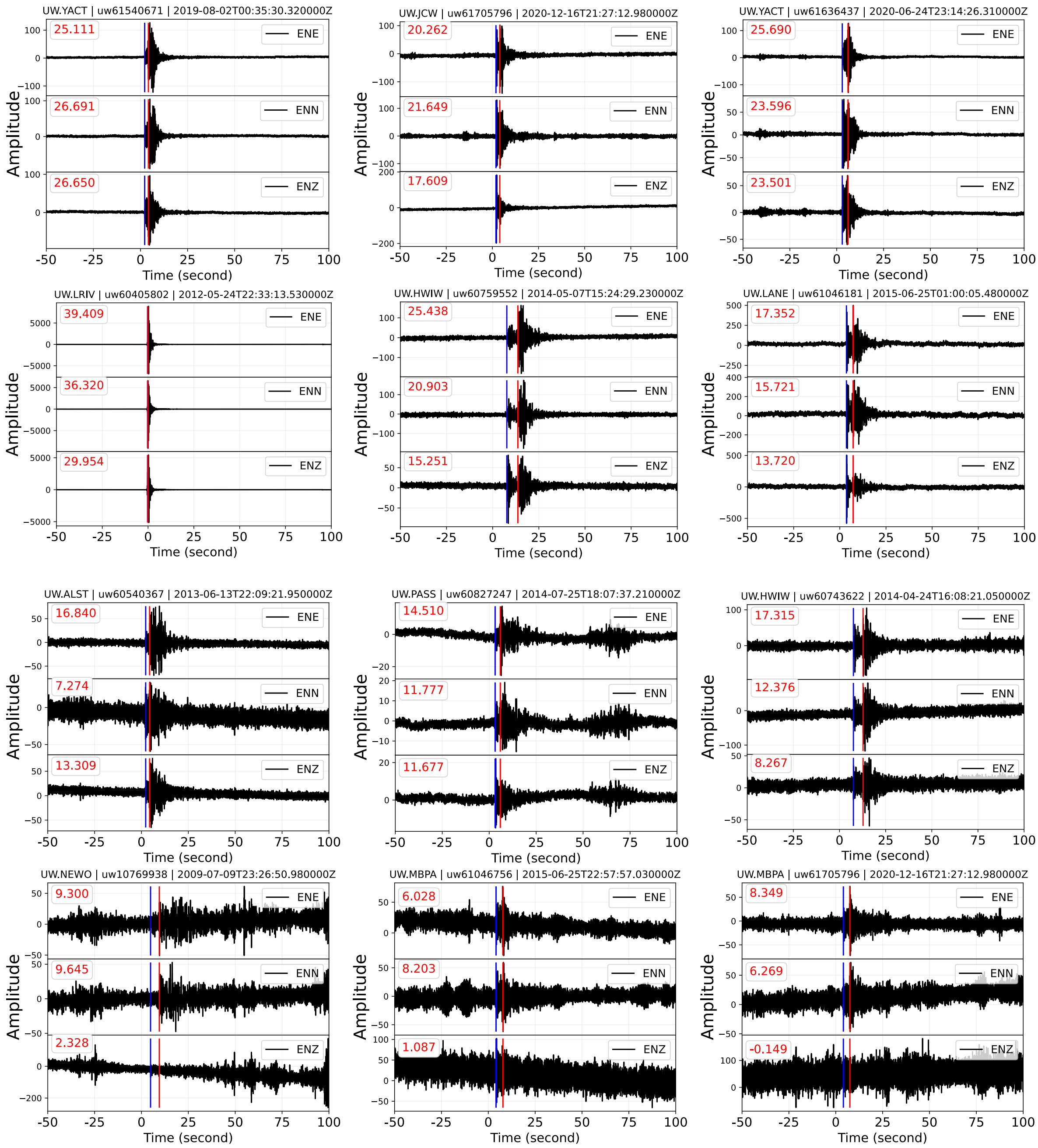

Figure S24 Randomly selected waveform samples of ComCat explosion events from strong-motion EN? channels. SNRs are marked on the upper left for each component. The blue line marks the P-wave arrival, and the red line (if any) marks the S-wave arrival.

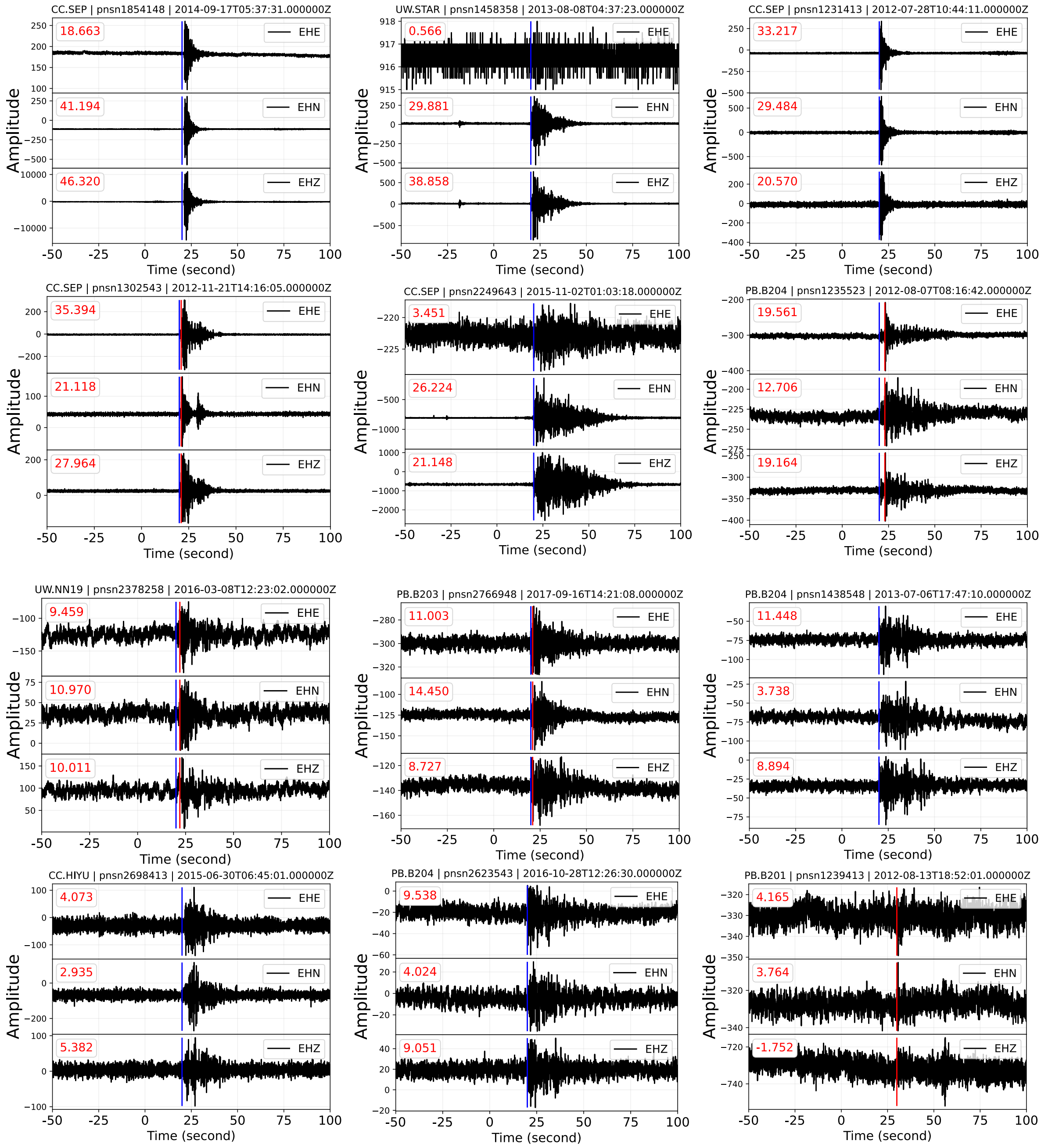

Figure S25 Randomly selected waveform samples of exotic surface events from short-period three-component EH? channels. SNRs are marked on the upper left for each component. The blue line marks the P-wave arrival, and the red line (if any) marks the S-wave arrival.

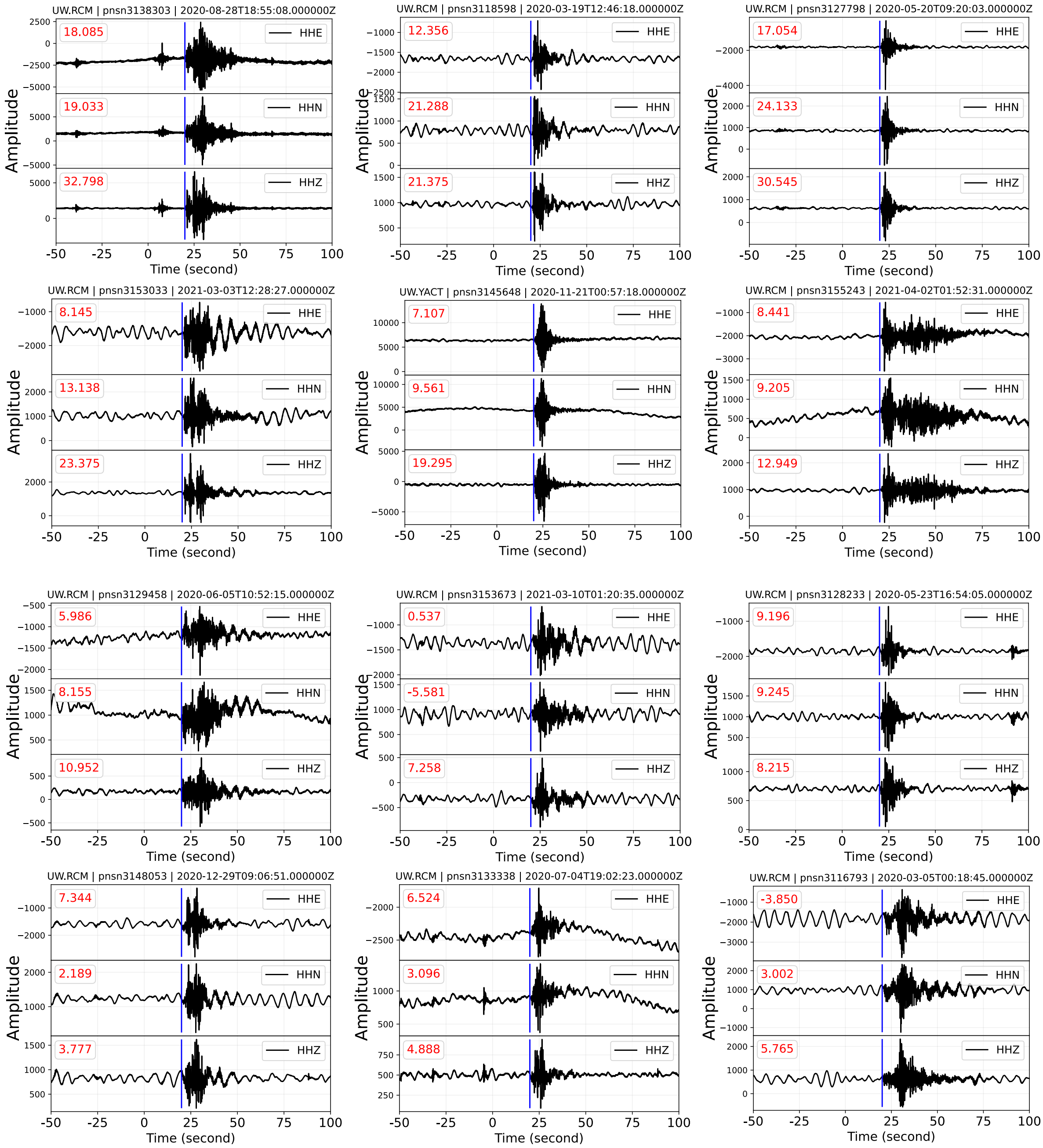

Figure S26 Randomly selected waveform samples of exotic surface events from board-band three-component HH? channels. SNRs are marked on the upper left for each component. The blue line marks the P-wave arrival, and the red line (if any) marks the S-wave arrival.

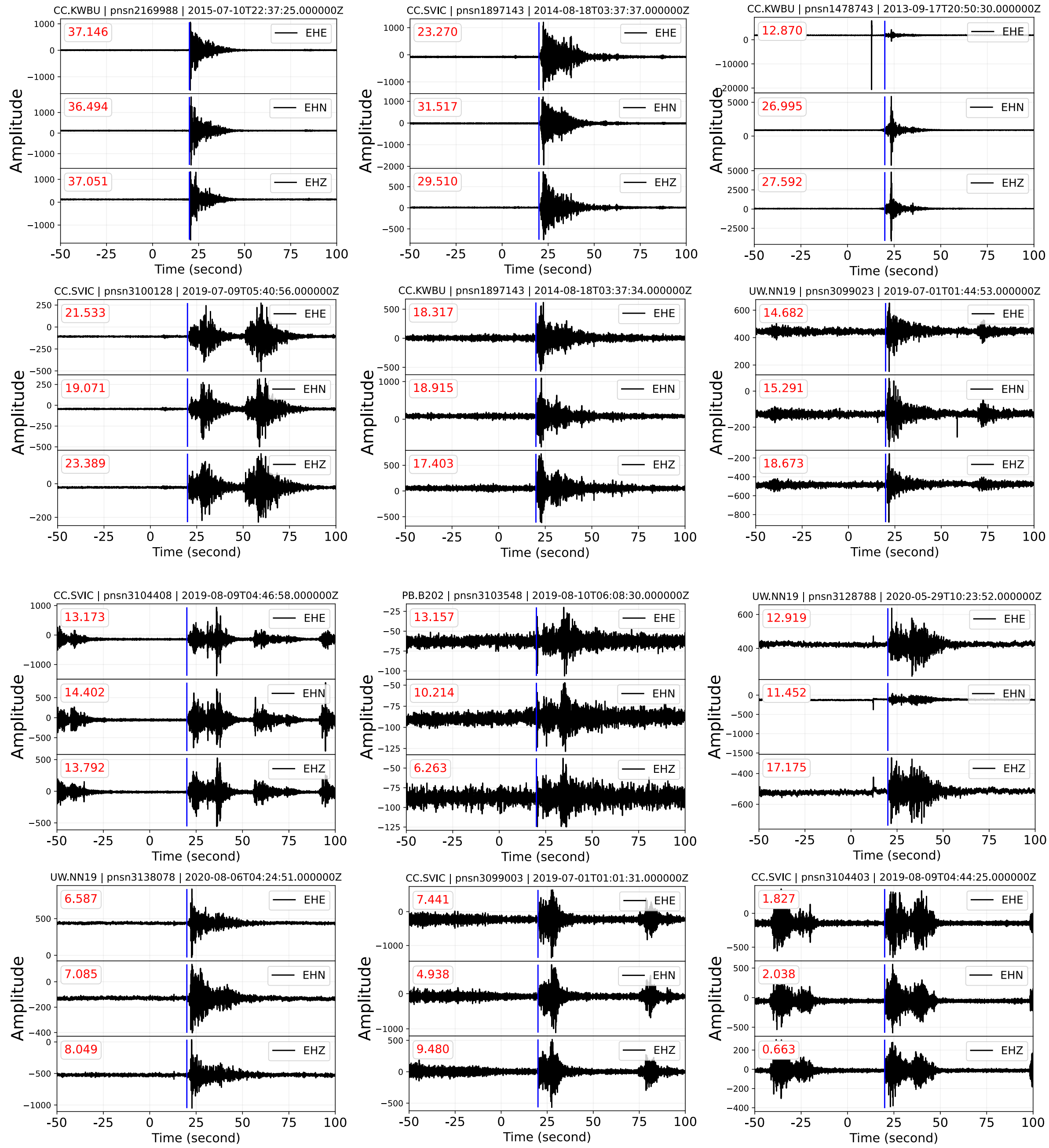

Figure S27 Randomly selected waveform samples of exotic thunder events from short-period three-component EH? channels. SNRs are marked on the upper left for each component. The blue line marks the P-wave arrival, and the red line (if any) marks the S-wave arrival.

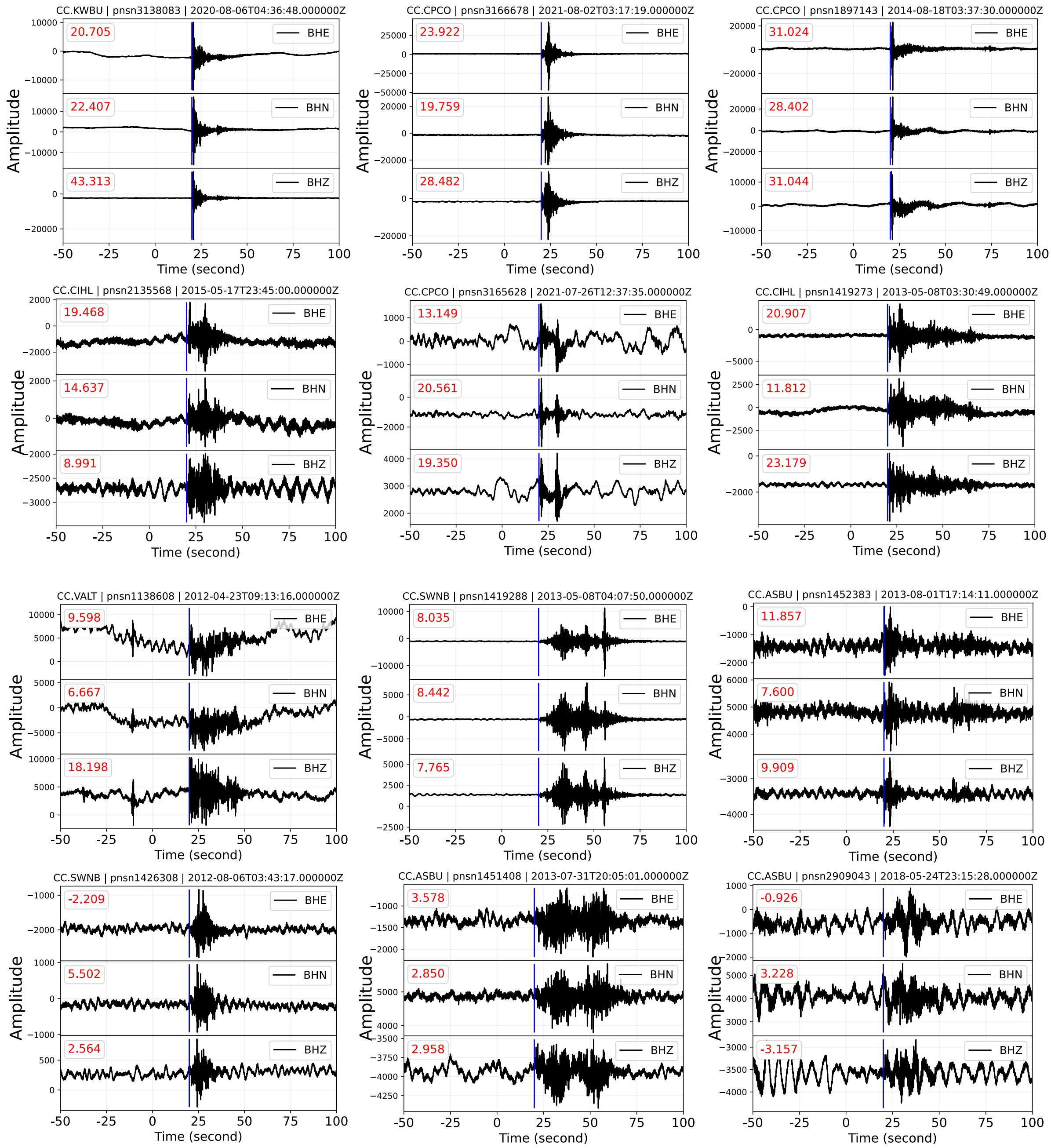

Figure S28 Randomly selected waveform samples of exotic thunder events from board-band three-component BH? channels. SNRs are marked on the upper left for each component. The blue line marks the P-wave arrival, and the red line (if any) marks the S-wave arrival.

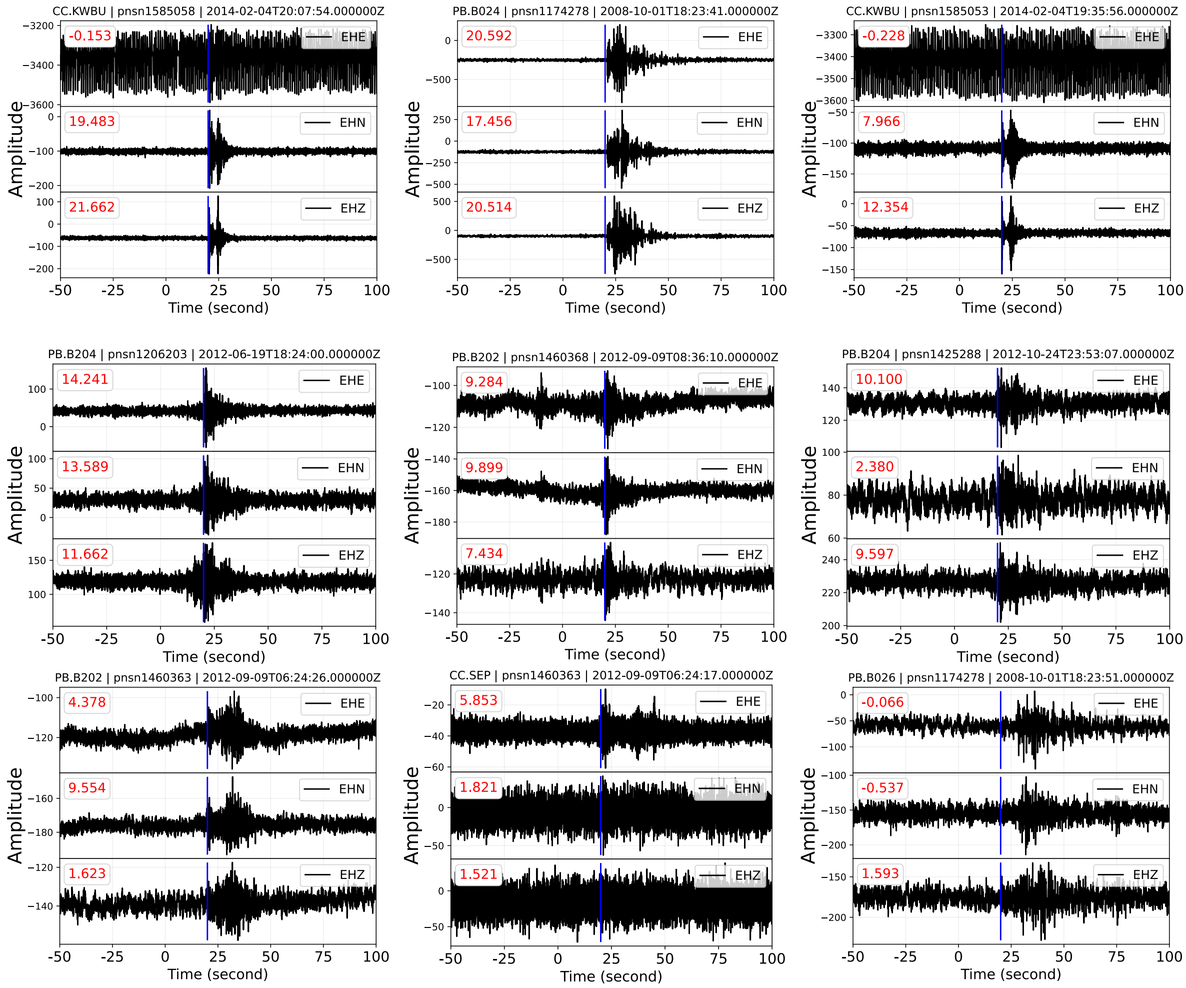

Figure S29 All waveform samples of exotic sonic boom events from short-period three-component EH? channels. SNRs are marked on the upper left for each component. The blue line marks the P-wave arrival, and the red line (if any) marks the S-wave arrival.

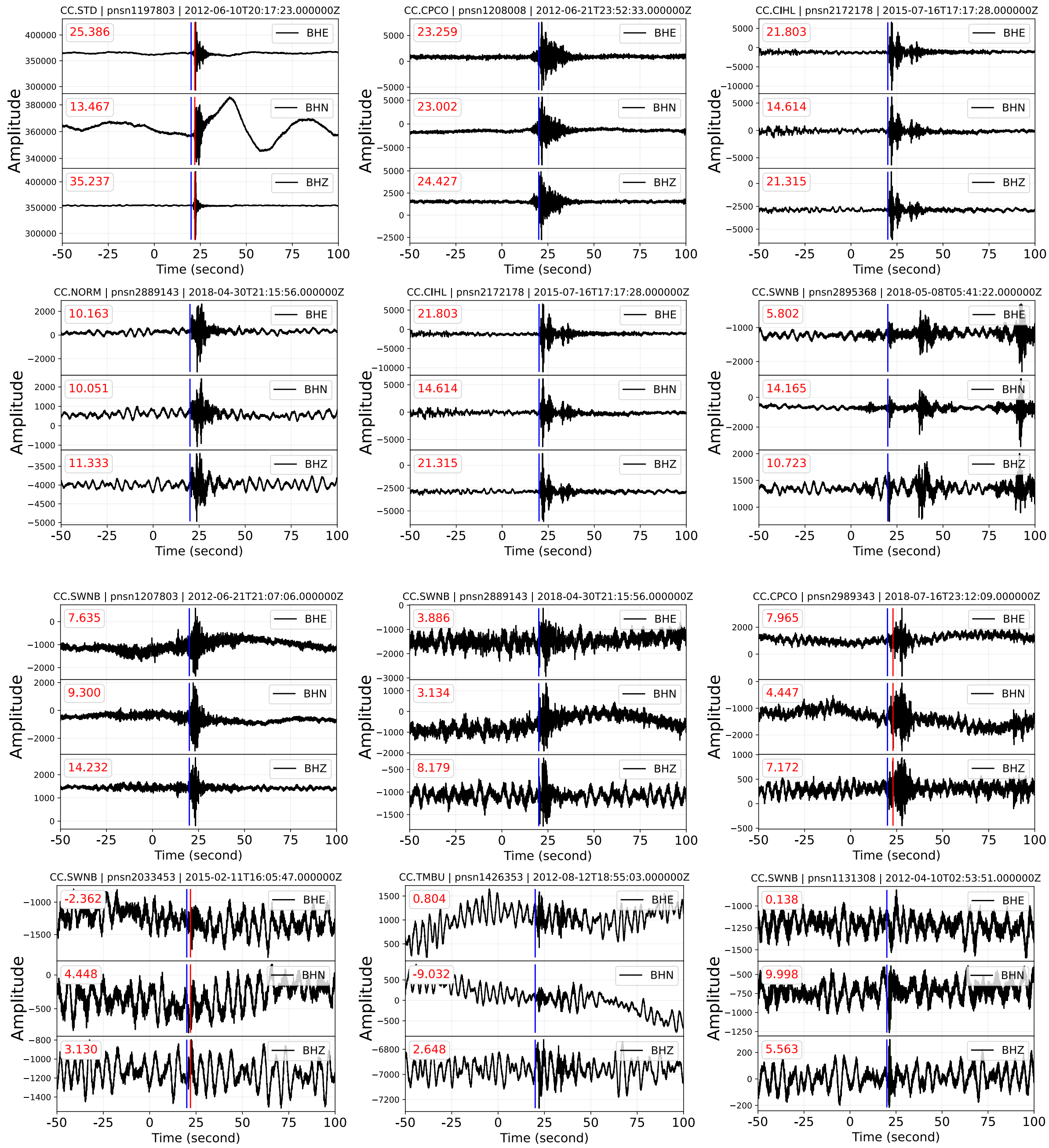

Figure S30 Randomly selected waveform samples of exotic sonic boom events from board-band three-component BH? channels. SNRs are marked on the upper left for each component. The blue line marks the P-wave arrival, and the red line (if any) marks the S-wave arrival.

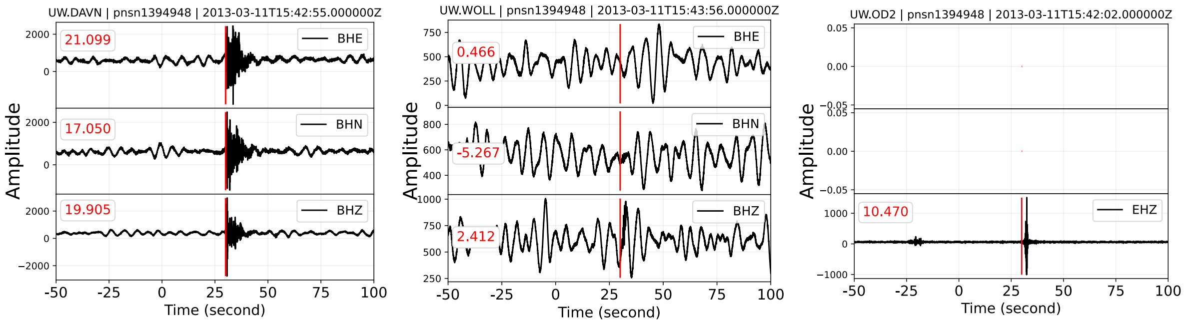

Figure S31 All waveform samples of exotic plane crash events. SNRs are marked on the upper left for each component. The blue line marks the P-wave arrival, and the red line (if any) marks the S-wave arrival.

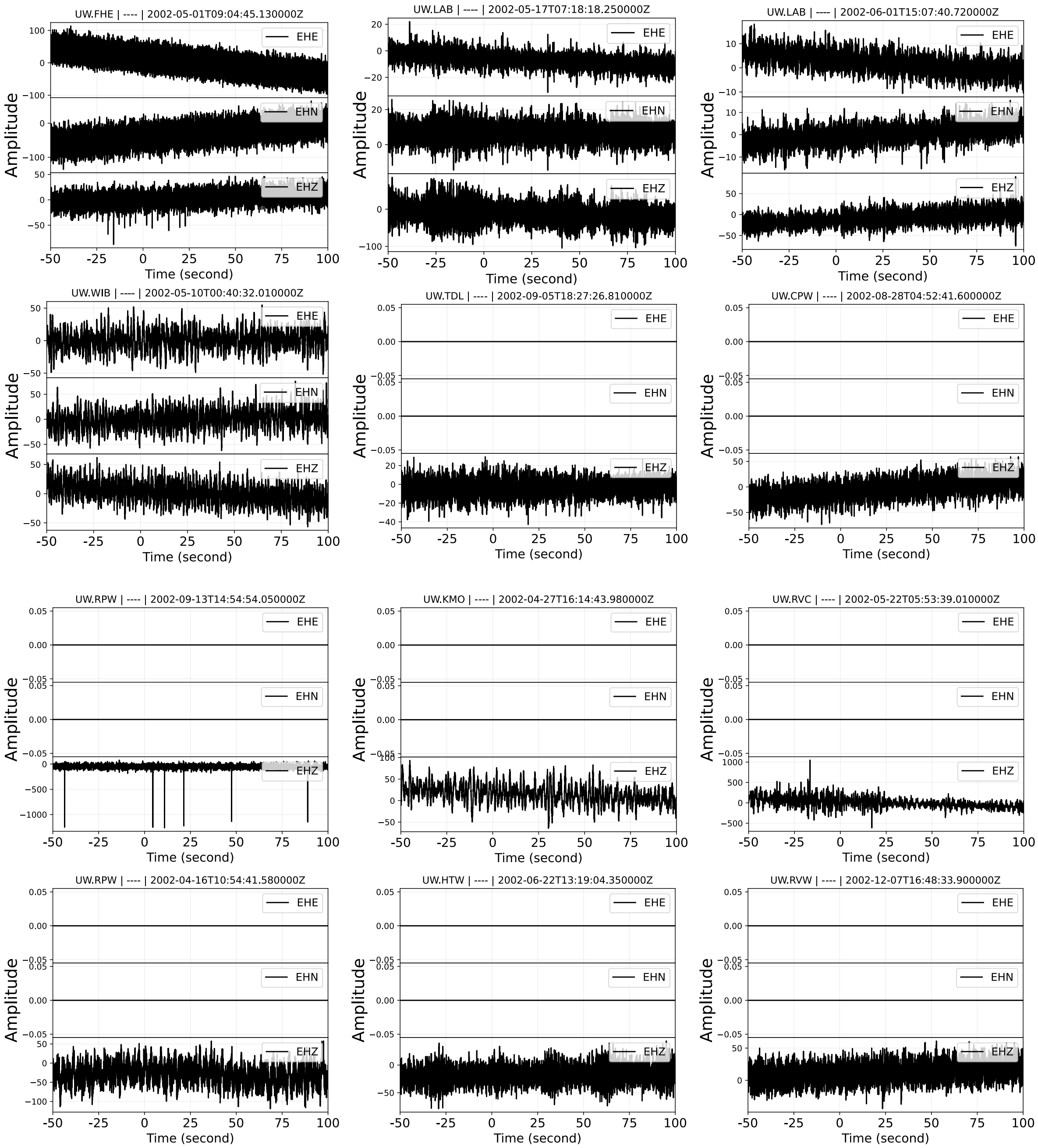

Figure S32 Randomly selected noise waveform samples from short-period EH? channels.

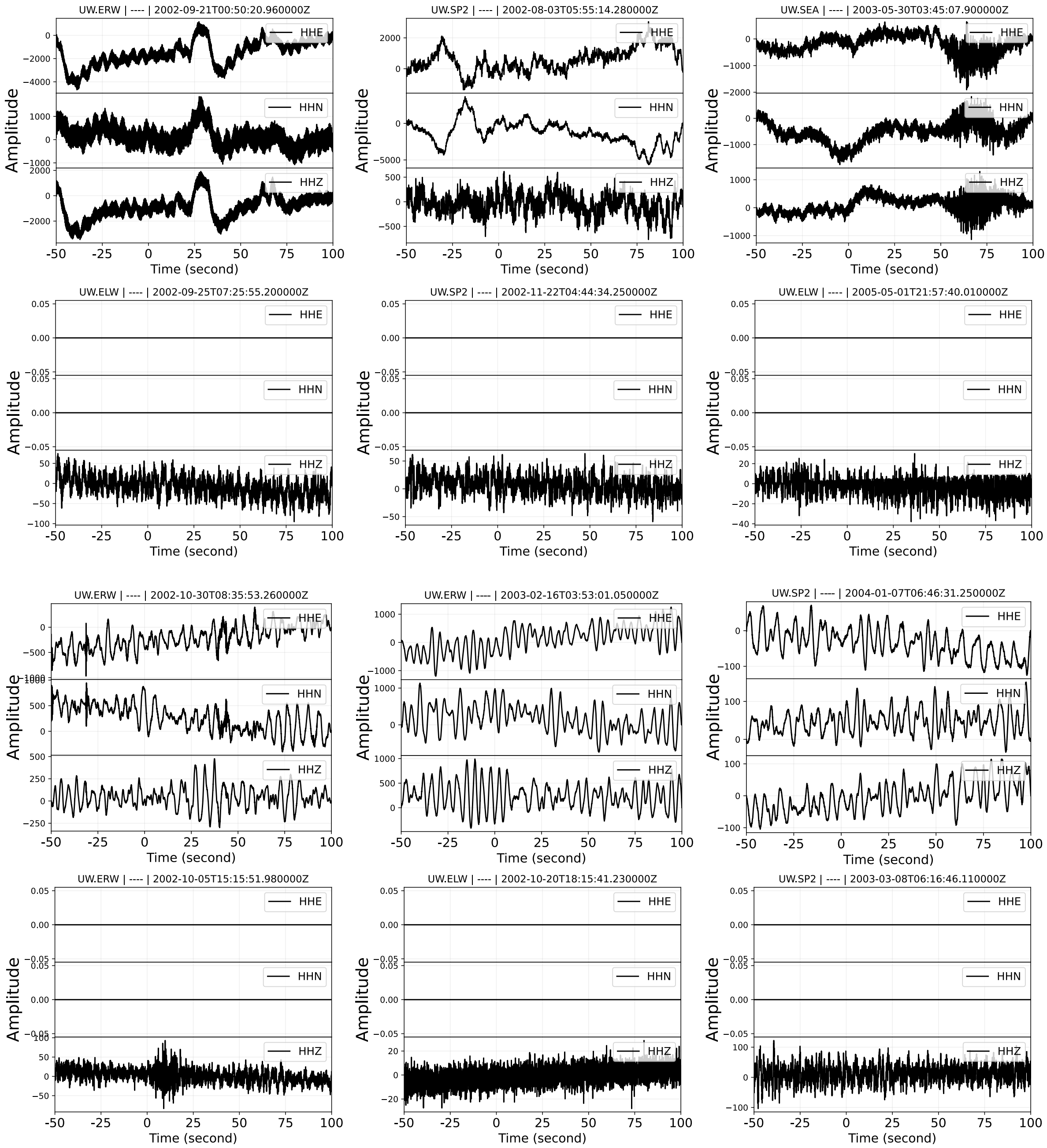

Figure S33 Randomly selected noise waveform samples from board-band three-component HH? channels.

References

Woollam, J., Münchmeyer, J., Tilmann, F., Rietbrock, A., Lange, D., Bornstein, T., Diehl, T., Giunchi, C., Haslinger, F., Jozinović, D., et al. Seisbench—a toolbox for machine learning in seismology. *Seismological Society of America*, 93(3):1695–1709, 2022. doi: 10.1785/0220210324.